

## Recovering Injected Astrophysics from the LISA Double White Dwarf Binaries

V. DELFAVERO,<sup>1</sup> KATELYN BREIVIK,<sup>2</sup> SARAH THIELE,<sup>3</sup> R. O'SHAUGHNESSY,<sup>4</sup> AND J. G. BAKER<sup>1</sup>

<sup>1</sup> *Gravitational Astrophysics Laboratory, NASA Goddard Space Flight Center, Greenbelt, MD 20771, USA*

<sup>2</sup> *McWilliams Center for Cosmology and Astrophysics, Physics Department, Carnegie Mellon University, Pittsburgh, PA 15213, USA*

<sup>3</sup> *Department of Astrophysical Sciences, Princeton University, Princeton, NJ 08544, USA*

<sup>4</sup> *Center for Computational Relativity and Gravitation, Rochester Institute of Technology, Rochester, New York 14623, USA*

(Dated: January 27, 2025)

### Abstract

We present the successful recovery of common envelope ejection efficiency assumed in a simulated population of double white dwarf binaries like those which may be observed by the future LISA mission. We simulate the formation of double white dwarf binaries by using the COSMIC population synthesis code to sample binary formation conditions such as initial mass function, metallicity of star formation, initial orbital period, and initial eccentricity. These binaries are placed in the **m12i** synthetic Milky-Way-like galaxy, and their signal-to-noise ratio for the LISA instrument is estimated, considering a Galactic gravitational wave foreground informed by the population. Through the use of Fisher estimates, we construct a likelihood function for the measurement error of the LISA-bright DWD binaries ( $\geq 20$  SNR,  $f_{\text{GW}} \geq 5\text{mHz}$ ), in their gravitational wave frequency ( $f_{\text{GW}}$ ) and chirp mass. By repeating this process for different assumptions of the common envelope ejection efficiency, we apply Bayesian hierarchical inference to find the best match to an injected astrophysical assumption for a fiducial population model. We conclude that the impact of common envelope ejection efficiency on the mass transfer processes involved in double white dwarf formation may be statistically relevant in the future observed LISA population, and that constraints on binary formation may be found by comparing simulated populations to a future observed population.

### 1. INTRODUCTION

In the past decade, the LIGO/Virgo/KAGRA collaboration has published the first observations of gravitational waves from compact binary mergers in the kilohertz frequency band (Abbott et al. 2016). These measurements probe populations of stellar mass binary black holes and neutron stars which electromagnetic observations cannot probe except by targeting X-ray emission from accreting binaries (Fabbiano 2006; Remillard & McClintock 2006; Miller-Jones 2014; Inoue et al. 2022; Fortin, Francis et al. 2023). In the 2030s, the Laser Interferometer Space Antenna (LISA) will be the first space-based gravitational wave interferometer (eLISA Consortium et al. 2013). LISA will be most sensitive in a lower gravitational wave frequency than its extant ground-based counterparts and will observe detached compact binaries, such as the Double White Dwarf (DWD) population in The Milky Way (Nelemans et al. 2001; Ruiter et al. 2010; Toonen et al. 2012; Korol et al. 2017, 2018; Lamberts et al. 2019; Breivik et al. 2020; Korol et al. 2022b; Hirai & Mandel 2022; Biscoveanu et al. 2023; Tang et al. 2024) .

The LISA Galactic DWD binaries will probe isolated binary evolution in the lower end of the stellar mass spectrum where most stars reside. Several million DWDs in The Milky Way and local group are expected to radiate gravitational waves in the LISA band, with the majority having overlapping frequencies that can be observed as a Galactic gravitational-wave foreground (e.g. Benacquista & Holley-Bockelmann 2006; Breivik et al. 2020; Staelens & Nelemans 2024; Hofman & Nelemans 2024). In addition to the Galactic foreground, is expected that LISA will discover tens-of-thousands of individually resolved DWDs in The Milky Way (e.g. Nelemans et al. 2001; Nissanke et al. 2012; Tang et al. 2024) and the local group (e.g. Korol et al. 2018; Roebber et al. 2020; Korol et al. 2020; Keim et al. 2023). In addition to isolated binaries, LISA will discover DWDs that have been formed either dynamically in environments like globular clusters (Willems et al. 2007; Kremer et al. 2018), or higher-multiplicity systems in the field of The Milky Way (e.g. Offner et al. 2023). However, the Type Ia supernova rate from merging DWDs in globular clusters may be as low as  $10^{-7}\text{yr}^{-1}$  in an environment

like The Milky Way (Kremer et al. 2020, 2021), compared to a  $10^{-3} \text{yr}^{-1}$  estimate for the Type Ia rates of Milky-Way-like galaxies (Frohmaier et al. 2018). Furthermore, the fraction of WD progenitor stars formed in stellar triples is measured to make up 20% or less of the stellar population (e.g. Offner et al. 2023). Thus, the majority of resolved DWDs discovered by LISA are expected to have been born in isolated binary systems. Because of this, we can use comparisons between the predicted and observed isolated binary populations to infer constraints on models of binary evolution and learn about the underlying astrophysical processes.

As proof of concept, comparable methods have been applied to interpret the population of sources identified by ground-based gravitational wave detectors. The LVK has published approximately ninety gravitational wave observations in the Gravitational Wave Transient Catalog (GWTC) (Abbott et al. 2019, 2021a; The LIGO Scientific Collaboration et al. 2021a; The LIGO Scientific Collaboration & The Virgo Collaboration 2021). The population of these observations informs us about the underlying population of merging compact binaries (The LIGO Scientific Collaboration et al. 2020, 2021b; Abbott et al. 2021b). These merger events are expected to form from specific formation channels, such as the isolated evolution of massive stellar binaries (Hurley et al. 2002; Eldridge et al. 2017; Giacobbo et al. 2017; Breivik et al. 2020; Belczynski et al. 2020; Broekgaarden & Berger 2021; Broekgaarden et al. 2021; Fragos et al. 2022; Stevenson & Clarke 2022; Delfavero et al. 2023), and various dynamic formation scenarios (Romero-Shaw et al. 2020; Fragione et al. 2020; Gayathri et al. 2022; Gamba et al. 2023); see Mandel & Farmer (2022) for a detailed review of formation channels. By comparing gravitational wave observations to the results of binary evolution population synthesis models, we can use Bayesian inference to learn about the underlying astrophysics (Zevin et al. 2021; Stevenson et al. 2017; Delfavero et al. 2023). Within the context of these ground-based instruments, previous studies have used synthetic populations of sources within an end-to-end calculation to assess how well these calculations can constrain source model parameters, a process we denote for brevity as “injection recovery” (see, e.g., Barrett et al. 2017; Wysocki et al. 2019; Zevin et al. 2021) and references therein.

In this paper, we adapt the Bayesian hierarchical inference methods used to infer constraints on the formation of massive compact binaries from the LVK observations (e.g. Delfavero et al. 2023) to study the formation of LISA Galactic DWD binaries. We choose to focus on common envelope evolution in this paper as it is not well

constrained by existing studies, and may have a powerful impact on the population of Galactic DWD binaries observable by LISA (Korol et al. 2022a). Furthermore, we demonstrate the recovery of an injected astrophysical assumption about the common envelope efficiency parameter from the population of Galactic DWD gravitational wave sources with resolved chirp mass estimates.

This paper is organized such that each section describes the methods pertaining to a stage of our investigation, as well as results pertaining to that stage. In section 2, we describe our methods for simulating the evolution of DWD binaries with the COSMIC binary population synthesis code. We explore the impact of common envelope ejection efficiency on different formation scenarios for DWD binaries. In section 3, we explore the star formation environments in a synthetic galaxy, and identify the subpopulation of DWD binaries observable by LISA for our selection of formation models. In section 4, we describe our Bayesian hierarchical inference methods and their impact on populations of those simulated binaries which could be resolved above the stochastic gravitational wave background of the galaxy. In Section 5, we adopt an alternative approach investigating the usefulness of the KL divergence statistic on the populations of resolved binaries, in recovering an injected formation model. Finally, in section 7, we summarize the impact of our results and suggest how it may inform ongoing and future studies.

## 2. SIMULATING A POPULATION OF GALACTIC DWD BINARIES

There are many uncertainties remaining in the evolution of stellar binaries, such as the initial binary fraction (Thiele et al. 2023) and various forms of mass transfer initiated by Roche overflow interactions. One such form of dynamically unstable mass transfer is common envelope evolution, where the atmosphere of a donor star expands beyond its Roche lobe such that both stars become immersed in a common envelope. The most accurate method for characterizing the efficiency of common envelope evolution (in ejecting orbital energy and angular momentum from the system) is currently debated by various groups (e.g. Ivanova 2011; Ivanova & Chaichenets 2011; Klencki et al. 2021; Wilson & Nordhaus 2022; Hirai & Mandel 2022; Stefano et al. 2023; Tang et al. 2024). If the common envelope prescription employed in the simulation of DWD binaries fails to describe the onset and outcomes of common envelope evolution, this may account for a mismatch between the properties of observed and simulated populations.

It has been proposed that gravitational wave observations are an effective way to probe models of binary

evolution and constrain these uncertain processes (Barrett et al. 2017; Belczynski et al. 2020; Thiele et al. 2023; Delfavero et al. 2023). The first step in predicting a population of observable DWD binaries in the LISA band is to use a population synthesis code to simulate a population of DWD binaries for an assumed set of astrophysical assumptions and initial binary parameter distributions. We perform these simulations for different kinds of DWD binaries with different Zero Age Main Sequence (ZAMS) metallicity assumptions, and considering the evolution of a Galactic population from the dawn of cosmic stellar formation to present day.

### 2.1. Binary Population Synthesis with COSMIC

We use COSMIC (Breivik et al. 2020; Breivik et al. 2021) to simulate populations of DWD binaries. COSMIC is an open-source rapid binary population synthesis suite that is based on the single star evolution ‘Hurley’ fits (Hurley et al. 2000) to the ‘Pols 1990’ (Pols et al. 1998) stellar evolution tracks and binary evolution algorithm of (Hurley et al. 2002).

The primary difference between COSMIC and other rapid population synthesis tools like SeBa, (Portegies Zwart & Verbunt 1996) MOBSE (Giacobbo et al. 2018), StarTrack (Ruiter et al. 2010) or COMPAS (Riley et al. 2022), is the use of the *match* statistic, an iterative population sampling criteria inspired by matched filtering techniques. Instead of implementing an adaptive importance sampling technique like STROOPWAFEL’s implementation in COMPAS (Broekgaarden et al. 2019), the *match* statistic allows us to continuously draw samples until the shape of density histograms of binary parameters (like mass and orbital period) in the selected population become numerically stable. For a detailed discussion of the *match*, see Breivik et al. (2020).

COSMIC classifies WD remnants by their chemical composition; Helium dominated WDs are labeled “He”, while Carbon/Oxygen dominated WDs are labeled “CO”, and Oxygen/Neon dominated WDs are labeled “ONe”. Following Thiele et al. (2023), we separately simulate the HeHe, COHe, and COCO combinations, and collectively simulate all systems with an ONe WD (labeled ONeX). In this work, we refer to these classifications (HeHe, COHe, COCO, and ONeX) as “kinds” of DWD systems. This is primarily so that the *match* criteria can accurately capture the mass distributions of each WD binary class. In the case of ONeX binaries, however, the number of these systems formed per unit solar mass of stars formed is significantly lower. Hence, we combine all companion WD classes for these binaries. Also following Thiele et al. (2023), we simulate populations of each type of DWD in 15 metallicities,

distributed uniformly in the log-space of the interval  $[10^{-4}, 0.03]$ , consistent with the limits of the Hurley fits to the Pols stellar evolution tracks (Pols et al. 1998; Hurley et al. 2000, 2002).

The primary mass of each binary is sampled from a Kroupa 2001 IMF (Kroupa & Weidner 2003), while the secondary is drawn from a uniform distribution in mass ratio ( $q \in [0.01, 1.0]$ ). COSMIC assumes a metallicity-dependent close binary fraction (i.e. fraction of stellar binaries with initial orbital periods less than six days) consistent with Moe et al. (2019) that decreases from 50% at  $Z=0.0001$  to 15% at  $Z=0.02$ . The orbital periods are distributed log-normally with increased numbers of systems below 10,000 days at sub-solar metallicities. We further assume that initial orbital eccentricities are uniformly distributed between 0 and 1.

Model ID	sampling	$\alpha_{\text{CE}}$
CEb50-CEb70	linear	[0.5, 1.5]
CEb71-CEb81	logarithmic	[0.1, 10.]

**Table 1. Common envelope assumptions for COSMIC models:** The label and corresponding value of  $\alpha_{\text{CE}}$  for each model included in this study. For reference, CEb60 is our model for  $\alpha_{\text{CE}} = 1.0$ .

COSMIC contains several updated prescriptions that treat binary-star interactions. For a detailed discussion of these updates, see Breivik et al. (2020). We broadly apply the default assumptions for binary interactions as indicated in the documentation for V.3.4.10 of COSMIC.

As noted by Thiele et al. (2023), assumptions for common envelope evolution can play a significant role in the size and characteristics of the DWD population. In this work, we use an energy conservation argument (e.g. Paczynski 1976) that balances the binding energy of the envelope with the change in orbital energy required to eject the envelope. In this case, we use the common envelope ejection efficiency,  $\alpha_{\text{CE}}$  to characterize this process, and allow it to vary broadly in order to avoid the exclusion of models which account for phase transitions and other astrophysical effects. The case where  $\alpha_{\text{CE}} = 1$  represents a perfect conversion of the orbital energy reservoir to be used in unbinding the envelope. We assume that the binding energy of the envelope, often characterized by a  $\lambda$  parameter, is modeled based on the envelope structure of the donor (as described in Appendix A of Claeys, J. S. W. et al. 2014). We note that  $\alpha_{\text{CE}}$  and  $\lambda$  parameters enter into our common envelope ejection model as

$$\frac{E_{\text{bind},i}}{\lambda} = \alpha_{\text{CE}}(E_{\text{orb},i} - E_{\text{orb},f}). \quad (1)$$

Thus, by keeping our binding energy model assumptions fixed, changes in  $\alpha_{\text{CE}}$  may be equivalently capturing different descriptions for the binding energy parameter  $\lambda$ . Indeed, the case of  $\alpha_{\text{CE}} > 1$  could be due to additional energy sources or due to donors with less bound envelopes than our model assumptions (Yamaguchi et al. 2024b,a).

For common envelope evolution, the binding energy in the implementation of COSMIC we use here is estimated as in Appendix A of Claeys, J. S. W. et al. (2014). For the common envelope ejection efficiency ( $\alpha_{\text{CE}}$ ), we assume a small family of models with values ranging logarithmically between 0.1 and 10, and a more finely sampled family of models with values ranging linearly between 0.5 and 1.5 (see Table 1). We chose these values to bracket the wide uncertainty associated with common envelope ejection, though we note that multiple studies have found ejection efficiencies near  $\alpha_{\text{CE}} \sim 0.3$  for WD binaries (e.g. Zorotovic et al. 2010; Scherbak & Fuller 2023) or a potential scaling of  $\alpha_{\text{CE}}$  with the mass of the donor star (e.g. De Marco et al. 2011). Our results include 480 COSMIC simulations of DWD populations (for 32 choices of  $\alpha_{\text{CE}}$  and 15 choices of ZAMS metallicity). Both CEB60 and CEB76 have  $\alpha_{\text{CE}} = 1.0$ , where CEB60 is considered our fiducial (or injected) population and CEB76 was used to examine the impact of random number generation within COSMIC on statistical inference.

## 2.2. Gravitational wave evolution and delay time

All close DWD binaries shrink due to gravitational wave radiation from the time of DWD formation to present day. The LISA binaries will also shrink during the lifetime of the LISA mission. Orbital evolution due to gravitational wave radiation in a circular binary is carried out using the definitions from Peters (1964):

$$a_f = (a_i^4 - 4\beta t_{\text{delay}})^{1/4} \quad (2)$$

$$\beta = \frac{64G^3}{5c^5} m_1 m_2 (m_1 + m_2), \quad (3)$$

where  $a_i$  and  $a_f$  are the initial and final separation of the binary, and  $m_1$  and  $m_2$  are the mass of each object.

Ultimately, the quantities which describe potential gravitational wave observations are masses and orbital periods. These are related to the star forming conditions via a delay time: the time between the zero age main sequence formation of the binary and a gravitational wave observation. To track this evolution properly, we characterize each binary by the separation and mass of each remnant at the time of the formation of the white dwarf. As DWD orbital frequencies continue to evolve over time according to gravitational wave radiation, we

calculate this “delay time” as the sum of the time required to form the compact binary ( $t_{\text{form}}$ ) and the time required to evolve the system to a final orbital frequency at present day ( $t_{\text{evol}}$ ). Therefore, we draw several quantities from the output of COSMIC simulations: the separation of the binary at DWD formation, the mass of each remnant, and the time of compact binary formation. Because Roche lobe overflow is assumed to fully circularize close DWDs, which are the products of either stable mass transfer or common envelope, all DWD binaries analyzed in this work are assumed to form as circular binaries. We also interpret COSMIC outputs to track the prevalence of different chemical compositions in the underlying white dwarf populations.

Gravitational wave radiation can drive some binaries to transfer mass or contact before present day. These systems can exchange mass or merge during the DWD stage of a binary’s life. For these systems, the “delay time” is the time between star formation and contact (rather than between star formation and present day). The fate of such a system can be hard to determine given our current state of knowledge, but may depend on many things including the mass ratio of the binary (Marsh et al. 2004; Gokhale et al. 2007; Sepinsky et al. 2010; Kremer et al. 2015; Kremer et al. 2017). While these binaries may be observable by LISA, they will be identified separately from the detached binary population (Breivik et al. 2018), and we consider them beyond the scope of this work. Our assumptions about how close a DWD binary must come (i.e. the critical separation) before mass transfer may occur are consistent with Thiele et al. (2023).

On the other hand, some binaries may remain too wide to fall inside of LISA’s sensitivity. In this work, we consider DWD binaries with frequencies that satisfy  $f_{\text{GW}} \in [10^{-4}, 1.0]\text{Hz}$  at the present day, consistent with LISA’s nominal sensitivity requirements (Colpi et al. 2024).

Section 3.2 explores which binaries will have resolved parameter estimates, and which will contribute to the Galactic foreground.

## 2.3. Results of changing $\alpha_{\text{CE}}$ on binary formation pathways

For each COSMIC simulation, we obtain both the number of DWDs of a given kind ( $N_{\text{DWD,sim}}(\mathcal{Z}, \text{kind})$ ) and the total mass of all binaries sampled ( $M_{\text{ZAMS,sim}}(\mathcal{Z}, \text{kind})$ ) to produce the DWDs in our simulated population. This allows us to estimate the formation efficiency of DWDs per unit solar mass of star

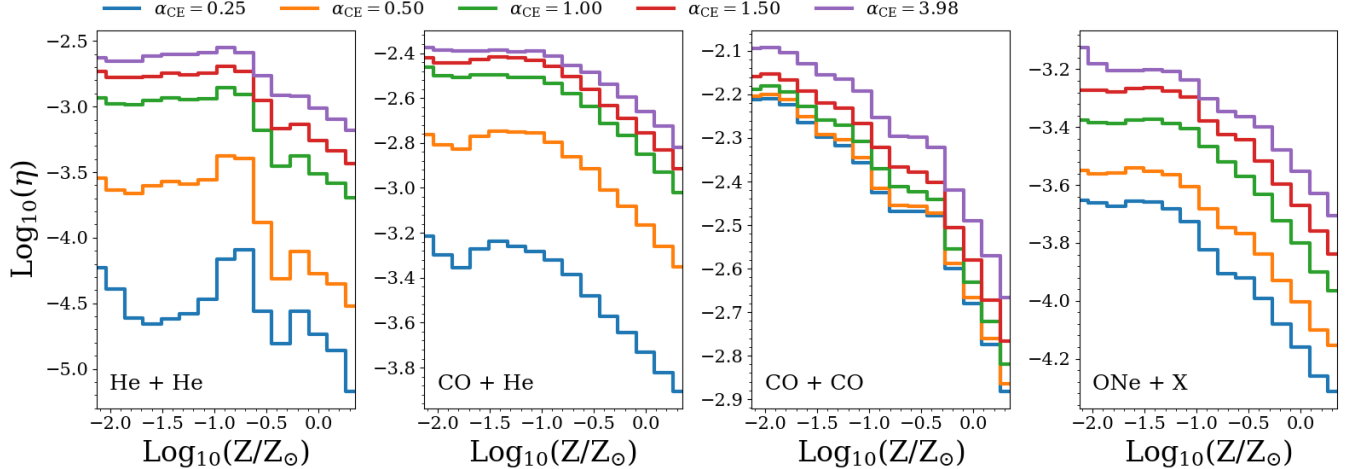


**Figure 1. The DWD formation efficiency as a function of metallicity:** Each curve represents the number of DWDs which form per solar mass of star formation, for a given type of DWD and for a given metallicity. The color of each curve indicates the  $\alpha_{\text{CE}}$  assumption for a batch of COSMIC runs.

formation,

$$\eta_{\text{form}}(\mathcal{Z}, \text{kind}) = N_{\text{DWD},\text{sim}}(\mathcal{Z}, \text{kind}) / M_{\text{ZAMS},\text{sim}}(\mathcal{Z}, \text{kind}), \quad (4)$$

for each kind of DWD binary (HeHe, COHe, COCO, ONeX), at each COSMIC metallicity.

Figure 1 exhibits the formation efficiency of DWD binaries for a few choices of  $\alpha_{\text{CE}}$ , selected to encompass the range of all simulated alphas. We note that as  $\alpha_{\text{CE}}$  increases,  $\eta_{\text{form}}$  increases as well; broadly, this is because fewer systems undergo pre-DWD stellar mergers when common envelope ejection is more efficient. We point the reader to Section 5 of Thiele et al. (2023) for a related discussion of formation efficiency trends. We also note that this scaling is not applied uniformly across all kinds of DWD binaries and metallicities (note the varied y-axis ranges in Figure 1). The common envelope ejection efficiency has a stronger impact on binaries containing He WDs because their progenitors have smaller radii relative to CO or ONe WD progenitors. This means that the common envelopes which produce He WDs occur in orbits with initially shorter periods and thus a smaller orbital energy well to be used in unbinding the envelope from the system. As the common envelope ejection efficiency decreases, we find a significant reduction in the number of DWDs containing He WD due to mergers caused by unsuccessful envelope ejection. This motivates a search for further quantitative (statistical) dependence on  $\alpha_{\text{CE}}$  through i) the total number of binaries, ii) the relative contribution of different formation pathways to the overall population, and iii) the shape of the density in observable quantities.

### 3. A SYNTHETIC GALAXY OF LISA SOURCES

In order to simulate a LISA population of DWD binaries, we need to assume a star formation history by sampling from star formation in a synthetic galaxy. We fill this synthetic galaxy with binaries simulated by COSMIC to construct a Galactic DWD population. Following this, we classify binaries based on whether they have time to form and remain in the LISA band until present day. Finally, the binaries resolved above the confusion limit are identified from the sample population and their uncertainties are estimated using a Fisher matrix method with the *ldasoft* code (Littenberg et al. 2020).

#### 3.1. Sampling star formation with FIRE-2 *m12i*

In this work, we follow Thiele et al. (2023), and sample star formation from a Milky-Way-like synthetic galaxy, **m12i** (Wetzel et al. 2016), using the Feedback In Realistic Environment 2 (FIRE-2) simulations (Hopkins et al. 2014; Hopkins 2015; Hopkins et al. 2018). This simulated galaxy was generated using the GIZMO code (Hopkins 2015) to solve hydro-dynamical equations and evolve Galactic morphology and star formation incorporating stellar feedback and metallicity evolution across cosmic time. The Latte suite of the FIRE-2 simulations follow the evolution of Milky-Way-like galaxies (such as **m12i**) (Wetzel et al. 2016; Garrison-Kimmel et al. 2017; Sanderson et al. 2020).

The star formation history of the **m12i** synthetic galaxy is represented by discrete packets of star formation, henceforth referred to as “star particles”. Each star particle represents  $7070M_{\odot}$  of star formation. The star particle samples from the database for **m12i** include local satellite galaxies. Consistent with Lamberts et al.

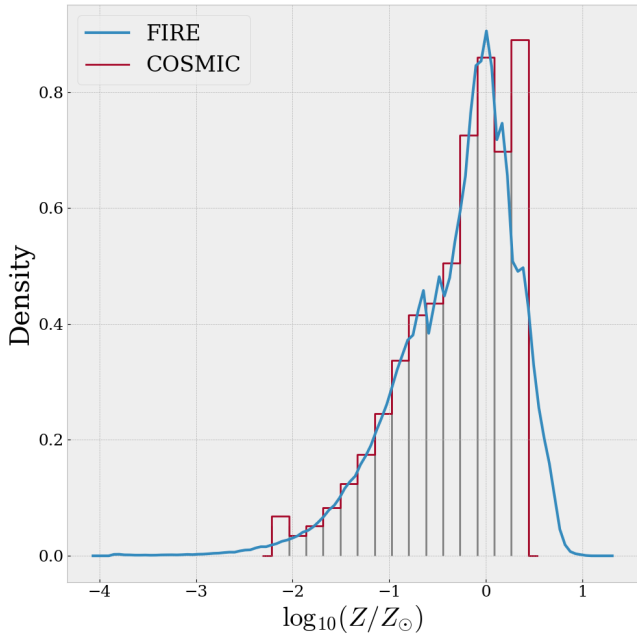


**Figure 2. Sampling from discrete metallicity bins:** The DWD populations are simulated on a fixed grid of metallicities, and the FIRE-2 star particles have a metallicity distribution which varies continuously. Therefore, each star particle must be sorted into the closest COSMIC metallicity bin. This figure features histograms for both the FIRE star particle metallicities (100 bins) and the 15 COSMIC metallicity bins. This figure demonstrates an example for the CEB60 model ( $\alpha_{\text{CE}} = 1.0$ ), in order to broadly contrast the continuous and discrete metallicity distributions.

(2019), we distinguish our central galaxy by defining as selection within 300kpc of the center of the galaxy. In practice there is no need to enforce this selection, as there are no DWD systems outside of this region which meet the LISA signal-to-noise-ratio cut we use to define the resolved population (see Section 3.2).

We use the time of star formation, the metallicity, and position of each star particle to assign formation times and positions for binaries simulated by COSMIC. We sort these into metallicity bins, corresponding to the closest discrete COSMIC simulation metallicity (see Figure 2). We estimate the number of binaries per star particle for each metallicity bin, according to our formation efficiency (Eq. 4):  $N_{\mathcal{Z}, \text{kind}} = \eta_{\text{form}}(\mathcal{Z}, \text{kind}) M_*$ , where  $M_*$  is the mass of a star particle ( $7070 M_\odot$ ). For each star particle, the number of samples drawn from the corresponding COSMIC simulation starts at the integer portion of  $N_{\mathcal{Z}, \text{kind}}$ , with an additional sample being drawn a fraction of the time equal to the decimal portion.

Previous work (Thiele et al. 2023) used the Ananke framework (Sanderson et al. 2020) to populate the **m12i**

galaxy with DWD systems, offset to the center of each star particle by a random distance. In this work, we use the output from the Latte simulations directly, and note that for our fiducial model there are close to (or less than) one LISA-band DWD binary for each star particle. We therefore populate the galaxy with DWD binaries at the center of each star particle.

Within COSMIC, solar metallicity ( $\mathcal{Z}_\odot = 0.02$ ) is consistent with Tout et al. (1996), to which the radii and luminosity power-laws from BSE are calibrated. This Tout et al. (1996) metallicity assumption is a poor estimator of iron abundances, as elemental abundances are estimated from meteorites (Anders & Grevesse 1989). Meanwhile, in FIRE-2, solar metallicity is assumed to be  $\mathcal{Z}_\odot = 0.01342$ , calibrated to Asplund et al. (2009). For this reason, absolute metallicity (i.e. the base 10 logarithm of the fraction of elements with an atomic number of 3 or higher) of **m12i** star particles is used to inform this metallicity-dependent sampling process, as using different solar metallicity assumptions for FIRE-2 and COSMIC star formation can otherwise introduce a bias.

### 3.2. Confusion Limited Sources

We use LEGWORK (Wagg et al. 2022) to calculate the strain amplitude of each source in the second orbital frequency harmonic for the LISA instrument, assuming a LISA observation time of 4 years (see Section 3 of Thiele et al. 2023). We then use lidasoft (Littenberg et al. 2020) to estimate the Signal-to-Noise-Ratio (SNR) of each source above the Galactic foreground. With lidasoft, we analyze the LISA time domain interferometry across the AE channels, and estimate the confusion noise using a running median across frequency bins with a resolution determined by  $1/T_{\text{obs}} = 1/4\text{yr}^{-1} \approx 8 \times 10^{-9}\text{Hz}$ . As well-resolved sources can be removed from the confusion of unresolved sources which make up the Galactic foreground, we subtract the brightest sources, recalculate the impact of the Galactic foreground on the population of resolved DWDs, and generate updated SNRs for each source. Finally, we also use lidasoft to estimate the inverse covariance matrix for high SNR ( $\geq 7$ ) sources using the Laplace approximation (Flournoy & Tsutakawa 1991; Cutler & Flanagan 1994). For the rest of this work, these sources are called the “resolved” population.

This approximation fits a Gaussian distribution to the posterior probability of each source:

$$P(\vec{\lambda}|\Lambda) \approx P(\vec{\lambda}|\Lambda)|_{\vec{\lambda}=\vec{\lambda}_*} \exp\left(-\frac{1}{2}(\vec{\lambda}-\vec{\lambda}_*)^T \Gamma^{-1}(\vec{\lambda}-\vec{\lambda}_*)\right), \quad (5)$$

where Fisher information  $\Gamma$  is given by

$$\Gamma^{-1} = -\nabla_{\vec{\lambda}} \nabla_{\vec{\lambda}} \ln(P(\vec{\lambda}|\Lambda)) \Big|_{\vec{\lambda}=\vec{\lambda}_*}, \quad (6)$$

and where  $\vec{\lambda}$  represents an arbitrary guess at the true parameters of a source,  $\vec{\lambda}_*$ , and  $\Lambda$  defines our other assumptions.

We use this Gaussian approximation to assume the form of our likelihood function  $\mathcal{L}(\vec{\lambda})$ , where our binary parameters are gravitational wave frequency ( $f_{\text{GW}}$ ), the time derivative of that frequency ( $\dot{f}_{\text{GW}}$ ), and strain amplitude ( $h$ ). Following this, we use the Jacobian transformation to change coordinates to  $f_{\text{GW}}$ , chirp mass ( $\mathcal{M}_c$ ), and distance ( $\ell$ ). We then marginalize over distance to construct a likelihood for each source,  $\mathcal{L}(f_{\text{gw}}, \mathcal{M}_c)$ . In gravitational wave Parameter Estimation (PE), Fisher estimates for parameter uncertainties can encounter numerical challenges, as well as bias (when astrophysical prior information is not fully considered). These and other limitations of Fisher estimates are summarized well by (Vallisneri 2008). However, as the number of sources can vary widely (up to tens of millions of sources), estimating a detailed likelihood approximation more detailed than a Fisher estimate for each source is beyond the scope of this work.

A reference prior is typically assumed for single-event parameter inference for the parameters of gravitational wave observations of massive compact binaries (Veitch et al. 2015; Ashton et al. 2019; Callister 2021). As this reference prior would factor out of our parameter estimates for synthetic DWD binaries, we do not need to adopt one.

### 3.3. Results of changing $\alpha_{\text{CE}}$ on Galactic binary populations

After sampling a Galactic DWD population from star formation assumptions for the **m12i** galaxy, we identify a Galactic binary population for each choice of our formation assumptions. We have explored 32 sets of COSMIC simulations with different choices for  $\alpha_{\text{CE}}$ . The assumed common envelope for each simulation can be found in Table 1.

The impact of common envelope efficiency on the number and classification of sources in the synthetic Galactic DWD population is demonstrated in Figure 3. This figure accounts for the close binaries within the LISA gravitational wave frequency band, those wide binaries which are outside of that band, and binaries which come close enough together to initiate mass transfer during the DWD phase. The number of LISA band sources can vary by orders of magnitude with different  $\alpha_{\text{CE}}$  assumptions. This is a direct consequence of models with

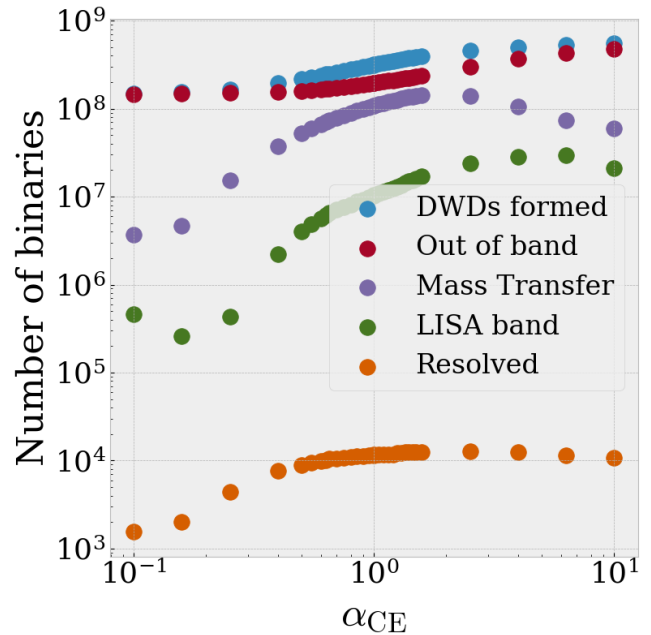


**Figure 3. Binary classifications in  $\alpha_{\text{CE}}$ :** Classifications of a simulated Galactic DWD population at different choices of  $\alpha_{\text{CE}}$ , for the **m12i** galaxy.

less efficient common envelope ejection leading to more stellar mergers that occur before a DWD can form (c.f. Figure 1).

We define the “LISA-bright” population as the sources with  $\text{SNR} > 20$ , and  $f_{\text{GW}} > 0.005$ . This population will be used for inference, to ensure strong PE results. After also applying the frequency cut, this SNR cut results in 1237 LISA-bright sources for our fiducial model (CEb60), and does not significantly reduce the number of LISA-bright sources compared to an SNR cut of 7, which would result in 1255 resolved sources. Figure 4 shows how the density of binaries (in their intrinsic parameters  $f_{\text{gw}}$  and  $\mathcal{M}_c$ ) changes with these cuts. It is worthy of note that the number of resolved and LISA-bright sources varies by fewer orders of magnitude than the total number of LISA band systems. This is because an increase in the number of LISA band sources causes an increase in confusion noise in the Galactic foreground, affecting sensitivity to individual sources.

The impact of common envelope ejection efficiency on the Galactic binary population extends further than just the number of predicted LISA-bright sources. Qualitatively, we observe subtle differences between the selected populations (see Figure 4). For example, the low  $\alpha_{\text{CE}}$  model lacks sources near the lower end of the mass range, and tends toward lower frequencies. This is because the lowest mass He WD progenitors interact in significantly closer binary configurations than their

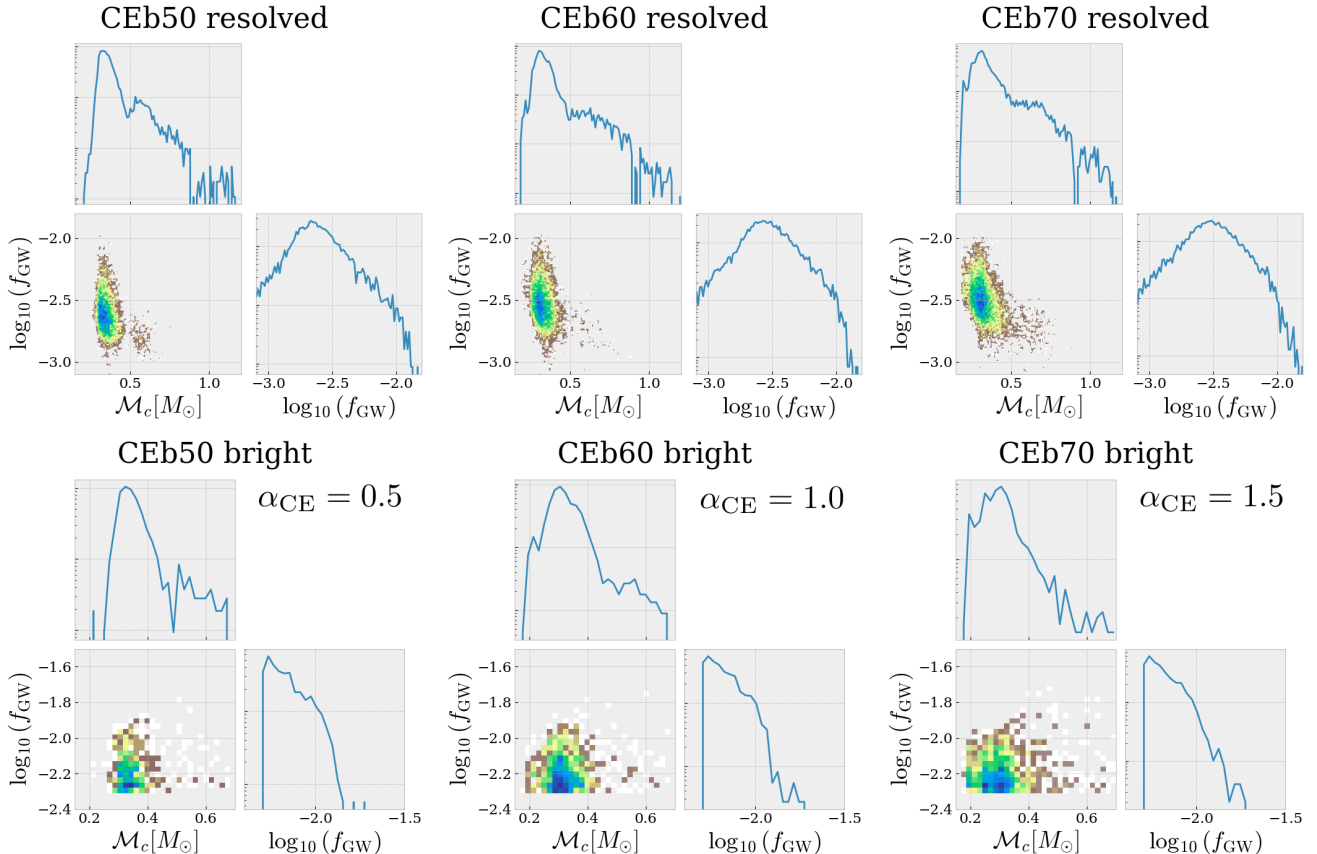


**Figure 4. Intrinsic parameters of the resolved population:** Each corner plot exhibits the one- and two-dimensional distribution for the resolved (top) or LISA-bright (bottom) population of Galactic DWD binaries, in  $\log_{10}$  of gravitational wave frequency and chirp mass. The resolved (top) plots identify sources for which  $\text{SNR} > 7$ . The LISA-bright (bottom) plots identify sources for which  $\text{SNR} > 20$  and  $f_{\text{gw}} > 5\text{mHz}$ . From left to right: CEB50 ( $\alpha_{\text{CE}} = 0.5$ ), CEB60 ( $\alpha_{\text{CE}} = 1.0$ ), and CEB70 ( $\alpha_{\text{CE}} = 1.5$ ) models. Each diagonal plot contains one-dimensional histograms for the intrinsic parameters, while the off-diagonal shows a two-dimensional histogram. Limits and bins are consistent across each row. Chirp mass is truncated at  $\mathcal{M}_c \leq 0.7M_{\odot}$ .

more massive counterparts. The orbital energy reservoir that is used in the common envelope ejection is thus much smaller. When combined with a lower common envelope ejection efficiency, these systems are more likely to merge prior to the formation of a DWD and thus not become LISA sources. For  $\alpha_{\text{CE}}$  greater than unity, we notice a distinct mode in the lower mass range that emerges due to these systems no longer merging before DWD formation. In the rest of this paper, we examine if these features are statistically robust enough to place common envelope model constraints using the LISA Galactic DWD population.

#### 4. HOW TO CONSTRAIN BINARY EVOLUTION MODELS WITH $\alpha_{\text{CE}}$

In the previous section, we identified our methodology for predicting a population of detached DWD binaries observable by LISA with resolved chirp mass estimates. By changing the assumptions of our binary evolution model, we can measure the impact of these assumptions

on predicted populations. Past work constraining populations of stellar mass black hole binaries using LVK observations has either made use of phenomenological population models or of likelihood models for individual observations constructed with the parameter estimation samples in the GWTC releases (Abbott et al. 2019, 2021a; The LIGO Scientific Collaboration & The Virgo Collaboration 2021; The LIGO Scientific Collaboration et al. 2021a; Collaboration & Collaboration 2021; Collaboration et al. 2021; Delfavero et al. 2021, 2022). In our own work, we have taken the latter approach (Delfavero et al. 2023). By integrating over the population of mergers predicted by binary population synthesis, past work was able to demonstrate a method for constraining the underlying assumptions in those population models.

We aim to demonstrate that in principle we can use the same approach to constrain LISA populations. In this work, we inject a population of LISA-bright DWD Galactic binaries with a known value of common envelope



lope ejection efficiency ( $\alpha_{\text{CE}}$ ), and attempt to recover  $\alpha_{\text{CE}}$  by comparing the injected population to test populations. We define the ‘‘LISA-bright DWD’’ population of a simulated galaxy (discussed in Section 2) to be those detached DWD binaries for which  $\text{SNR} > 20$  and  $f_{\text{gw}} > 5$  mHz, with covariance estimates from Fisher matrix approximations (described in Section 3.2).

Our approach relies on statistically characterizing how closely any test population resembles the injected population, both in count and properties. We estimate the likelihood of the injected data, given our population model. In this section, we detail the methods used to construct and evaluate the Inhomogeneous Poisson Point Process likelihood to draw constraints on injected astrophysics. We also discuss the role of marginalization over various realizations of a test population.

Finally, we demonstrate the effectiveness of this likelihood model through the example of a one-dimensional injection recovery in  $\alpha_{\text{CE}}$ .

#### 4.1. The Inhomogeneous Poisson Point Process likelihood

In general, when we run an experiment and measure some data,  $d$ , we can use Bayes’ theorem to evaluate the likelihood of some set of hypotheses,  $\mathcal{H}$ :

$$P(\mathcal{H}|d) = \frac{P(d|\mathcal{H})P(\mathcal{H})}{P(d)}. \quad (7)$$

where  $P(\mathcal{H}|d)$  is the posterior probability of our hypotheses,  $P(d|\mathcal{H})$  is the likelihood of our data given our set of hypotheses,  $P(\mathcal{H})$  is the probabilistic representation of our prior knowledge about  $\mathcal{H}$ , and  $P(d)$  is a marginalization factor to keep our probability distribution normalized. That marginalization factor can be calculated over all possible hypotheses:

$$P(d) = \int d\mathcal{H} P(d|\mathcal{H})P(\mathcal{H}). \quad (8)$$

Marginalization also allows us to reduce the dimensionality of our set of hypotheses: Suppose that our set of hypotheses depend on two parameters,  $\lambda_1$  and  $\lambda_2$ . We can also marginalize over  $\lambda_1$  to find our likelihood in terms of  $\lambda_2$ :

$$P(d|\lambda_2) = \int_{\lambda_1} P(d|\lambda_1, \lambda_2)P(\lambda_1)d\lambda_1. \quad (9)$$

In general, this also works if  $\lambda_1$  and  $\lambda_2$  are sets of parameters, rather than individual parameters. One can reduce the dimensionality of a model by integrating over the possible choices for a subset of the parameters which describe their set of hypotheses.

A counting experiment can be constrained as a Poisson Point Process, with a likelihood representing the possibility that an observed event count ( $N$ ) can occur, relative to the expected value of that event count ( $\mu$ ) according to a model. The Poisson likelihood is given by:

$$P(N|\mu) = \frac{\mu^N e^{-\mu}}{N!}. \quad (10)$$

Through Stirling’s approximation, one can arrive at the following expression for large numbers of sources:

$$\ln P(N|\mu) \approx N - \mu + N \times \ln(\mu/N). \quad (11)$$

The Inhomogeneous Poisson Point Process extends the treatment of a counting experiment, describing the likelihood for both the event rate, and the properties of a set of observations, compared to a given model (Moller & Waagepetersen 2003). This is especially useful when our observations ( $\{d_j\}$ ) have parameter uncertainties characterized by a source likelihood:

$$\mathcal{L}_j(\vec{\lambda}) = P(d_j|\vec{\lambda}, \Lambda). \quad (12)$$

Let the indices  $j$  and  $k$  refer to a sample binary from an observed (or injected) and modeled population respectively. The Inhomogeneous Poisson Point Process likelihood is the probability,  $P(\{d_j\}|\Lambda)$ , that the set of individual detections  $d_j$  could be observed under an assumed population model characterized by some assumptions  $\Lambda$ .

$$P(\{d_j\}|\Lambda) = \frac{\mu_\Lambda^N}{N!} e^{-\mu_\Lambda} \prod_j \left[ \int_{\{\vec{\lambda}\}} \mathcal{L}_j(\vec{\lambda}) \bar{\rho}_\Lambda(\vec{\lambda}) d\vec{\lambda} \right], \quad (13)$$

where  $\mu_\Lambda$  is the expected number of observations in the population model characterized by  $\Lambda$ ,  $N$  is the number of experimental (or injected) observations,  $\bar{\rho}_\Lambda(\vec{\lambda})$  is the normalized density of the population model in sample parameters  $\vec{\lambda}$ , and  $\mathcal{L}_j(\vec{\lambda})$  is the source likelihood.

The normalized density of a particular population model ( $\bar{\rho}_\Lambda(\vec{\lambda})$ ) is a kind of prior in  $\vec{\lambda}$ , and is often represented by a sufficiently large set of samples. We can evaluate the agreement of our observations to that model by integrating over that set of samples. It is therefore useful to approximate our specific realization of a continuously varying density function using samples from our binary evolution model with the Dirac Delta Function:

$$\bar{\rho}_\Lambda(\vec{\lambda}) = \frac{\sum_k^{N_\Lambda} \delta(\vec{\lambda} = \vec{\lambda}_k) w_k}{\sum_k^{N_\Lambda} w_k}, \quad (14)$$

where  $\Lambda$  describe a set of model assumptions,  $N_\Lambda$  is the number of samples in a population model described by

those assumptions,  $\vec{\lambda}_k$  are the parameters of a particular sample, and  $w_k$  is the weight given to a particular sample. In this work, we use equally weighted samples ( $w_k = 1.0$ ). Eq. 14 therefore simplifies to  $(1/N_\Lambda) \sum_k \delta(\vec{\lambda} = \vec{\lambda}_k)$ .

In practice, we calculate the logarithm of the Inhomogeneous Poisson Point Process likelihood, and have found it useful to distinguish the components of this likelihood. The component which measures the number of sources is the “rate likelihood.”

$$\ln P(N|\Lambda) = \ln(N - \mu_\Lambda) + N \times \ln(\mu_\Lambda/N). \quad (15)$$

The component which measures the shape of the observed parameter distribution is the “shape likelihood:”

$$\sum_j \ln P(d_j|\Lambda) = \sum_j \left[ \ln \left( \sum_k^{N_\Lambda} \mathcal{L}_j(\vec{\lambda}_k) \right) - \ln(N_\Lambda) \right]. \quad (16)$$

The “joint likelihood” is then the combination of these components (equivalent to Eq. 13):

$$\ln P(\{d_j\}|\Lambda) = \ln P(N|\Lambda) + \sum_j \ln P(d_j|\Lambda). \quad (17)$$

#### 4.2. Characterizing the likelihood of individual LISA-bright sources

In general, LISA-bright sources will be described by many parameters including astrophysical parameters (such as the gravitational wave frequency:  $f_{\text{gw}}$ ; the derivative of the gravitational wave frequency:  $\dot{f}_{\text{gw}}$ ; and the characteristic strain:  $h$ ), as well as extrinsic parameters such as sky location and orientation. In section 3.2, we described our process for constructing a likelihood estimate for each source in  $f_{\text{gw}}$ , chirp mass ( $\mathcal{M}_c$ ). By integrating over the sample population for the **m12i** galaxy in these parameters, we effectively marginalize over the extrinsic parameters (including sky location and phase).

When estimating the Inhomogeneous Poisson Point Process likelihood in this work, we use a multivariate normal distribution for each source ( $\mathcal{L}(\vec{\lambda}) = \mathcal{L}(f_{\text{gw}}, \mathcal{M}_c)$ ) of the injected LISA-bright DWD population. These multivariate normal distributions are truncated at  $f_{\text{gw}} = 0$  and  $\mathcal{M}_c = 0$ . We have obtained covariance estimates from the Fisher information about each source (see Section 3.2). In practice, these covariances are often fine enough that if we use them for our source likelihood model, it can be unlikely that any samples from the test population land where the likelihood for a particular source is substantially greater than zero.

In order to test the agreement of these populations effectively, we employ two strategies, we refine the likelihood model for our population in a couple of ways:

First, the contribution of any one source to the shape likelihood is cut off below  $\ln P(d_j|\Lambda) = -10$ . This prevents a stray binary in a strange part of parameter space from dominating the likelihood for the population. Second, the variance of each multivariate normal distribution is inflated (when appropriate) according to Scott’s rule for multivariate density estimation (Scott 2015):  $\sigma_{\text{Scott}} = n^{-1/(d+4)}$  where  $n$  is the number of samples and  $d$  is the number of dimensions.

Scott’s rule has been used historically to construct Kernel Density Estimates (KDEs) from a set of samples, where a multivariate normal distribution is constructed to estimate the contribution of each sample to the probability density. For now, we are not truly constructing a KDE, as we evaluate the likelihood on a source-by-source basis, our number of samples is determined by our Galactic population, the correlation between parameters is preserved, and because Scott’s rule only overrides the covariance estimates for which a smaller covariance was predicted by the Fisher information. Our likelihood model is a Gaussian Mixture Model (GMM), in the sense that it is sensitive to individual modes of the population (one for each source).

#### 4.3. A one-dimensional recovery of $\alpha_{\text{CE}}$ from an injected population

In this section, we explore the one-dimensional family of synthetic galaxies described in Section 3.3, in which  $\alpha_{\text{CE}}$  is the only formation parameter ( $\Lambda$ ) we vary (see 1 for the  $\alpha_{\text{CE}}$  value assumptions).

For a given value of  $\alpha_{\text{CE}}$ , we have up to 10 realizations of the **m12i** synthetic galaxy with different random number generator seeds. The differences between each realization include both the rotation of star particles (about the center of **m12i**) and the sampling of DWD binary populations. These differences are also formation parameters, and can be marginalized over by taking the average of likelihood values for all realizations with a given  $\alpha_{\text{CE}}$ . In practice, this marginalization favors the realization with the highest log likelihood (this is a mean in likelihood, not log-likelihood). Sampling from a uniform prior in the space of possible realizations allows us to minimize the impact of star formation sampling in our synthetic galaxy. This marginalization enables us to study the impact of formation parameters of interest without increasing the dimensionality of our effective formation parameter space.

For the LISA-bright DWD binaries, we’re not recording a number of instantaneous events in time, but we are still interested in counting the total number of sources identified in an injected population. In this work, we assume that the Inhomogeneous Poisson Point Process

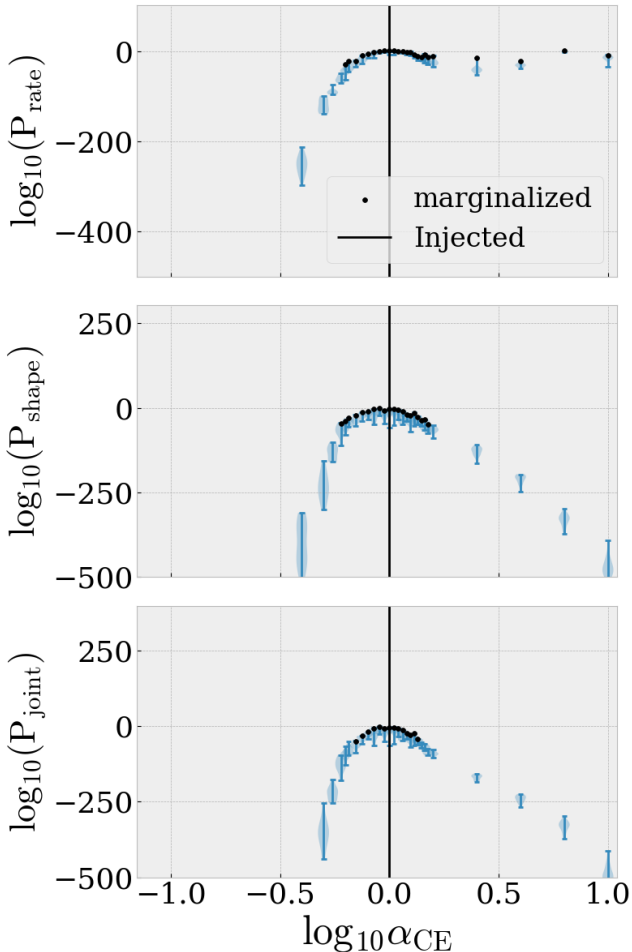


**Figure 5. The recovery of  $\alpha_{\text{CE}} = 1.0$  in a wide view:** By comparing the injected LISA-bright sources with test populations, we attempt to recover the injected  $\alpha_{\text{CE}}$  parameter using the Inhomogeneous Poisson Point Process likelihood model. The likelihood for several galaxy realizations for the each  $\alpha_{\text{CE}}$  value are shown in violin plots. Models are sampled sparsely in a logarithmic space where  $\alpha_{\text{CE}} \in [0.1, 10.0]$ , and linearly in  $\alpha_{\text{CE}} \in [0.5, 1.5]$ . Both sets of models are drawn here.

likelihood can be used to measure the agreement of an injected population of LISA-bright DWD binaries with test populations. We use the Inhomogeneous Poisson Point Process likelihood (Eq. 13) to evaluate the agreement of our injected sources with test populations.

By evaluating the agreement of our injected population at  $\alpha_{\text{CE}} = 1.0$  with each component binary of our test populations, we construct the likelihood in the space of  $\alpha_{\text{CE}}$  (see Figure 5). In this example, we see that the rate likelihood alone fails to effectively constrain  $\alpha_{\text{CE}}$ ; there is a local maximum near the injected value, but similar rates are observed far from that peak. However, the shape and joint likelihood of the population seem

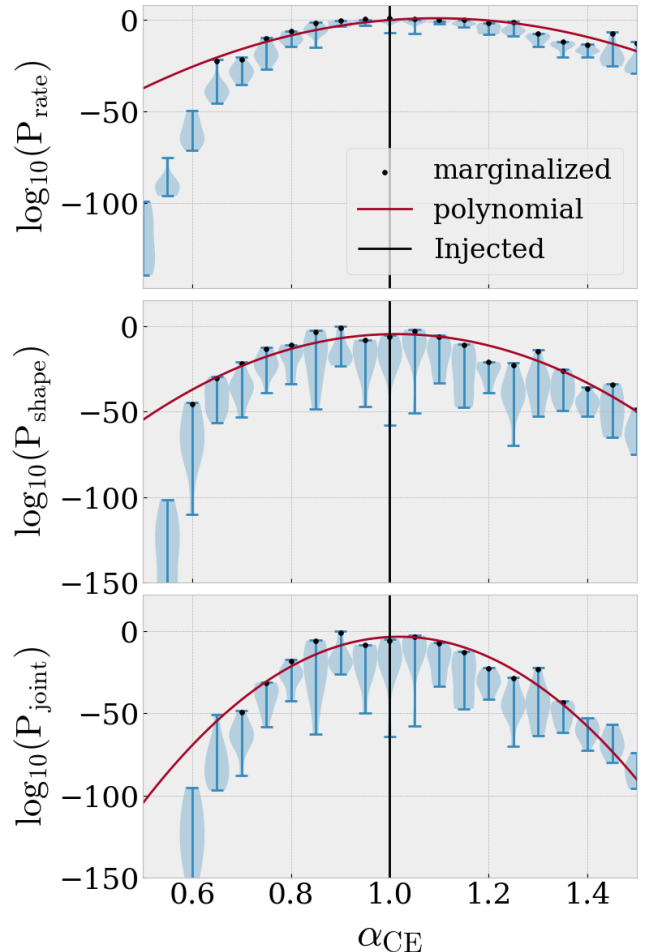


**Figure 6. The recovery of  $\alpha_{\text{CE}}$  in the vicinity of the peak:** The models highlighted in this zoomed in region are sampled linearly (with  $\alpha_{\text{CE}} \in [0.5, 1.5]$ ). Each likelihood model is characterized further by a quadratic (in log likelihood) in the vicinity of the peak.

to be unimodal on the wide scale given here (ranging several orders of magnitude in  $\alpha_{\text{CE}}$ ).

We take a closer look at each likelihood model in the vicinity of the injected value (Figure 6). Each likelihood model has a relative maximum in this region. Qualitatively, the joint likelihood seems to be the best predictor of the injected value. This should not be surprising when varying only  $\alpha_{\text{CE}}$ , as changes in the rate and shape of sample sources can both statistically be tied exclusively to common envelope physics. We take a more quantitative approach in Section 6.1.

## 5. CONSTRUCTING A KL DIVERGENCE STATISTIC FOR A POPULATION

In order to guarantee that we are constructing a minimally biased model, it is useful to use more than one statistic to characterize the agreement of our injected

population with test populations. In addition to the Inhomogeneous Poisson Point Process likelihood, we also use the Kullback-Leibler (KL) divergence (Kullback 1959) between two populations. We use the KL divergence to measure the information lost by assuming that a set of observations ( $p_*$ ) can describe a modeled population ( $p$ ). Similar to Section 4, we describe a particular population by a number of observations ( $\mu$  or  $\mu_*$ ) and a discrete set of samples which represent a density  $p(\vec{\lambda})$  or  $p_*(\vec{\lambda})$ . For the KL divergence approach, we characterize the density function with the  $\log_{10}(f_{\text{GW}})$  and  $\mathcal{M}_c$  binary parameters ( $\vec{\lambda}$ ).

### 5.1. The Kullback-Leibler divergence

Similar to the Inhomogeneous Poisson Point Process likelihood, the KL divergence between a tested population and reference population can be estimated with information about the rate of each population ( $D_{\text{KL}}(\mu_*|\mu)$ , for a number of observations  $\mu$ ), shape of each population ( $D_{\text{KL}}(p_*|p)$ ), or both ( $D_{\text{KL}}(p_*, \mu_*|p, \mu)$ ). We test the compatibility of a set of injected populations ( $p_*$ ) with several modeled populations ( $p$ ).

The KL divergence between our injected observations ( $p_*$ ) and a particular test model ( $p$ ) is defined by the asymmetric expression:

$$D_{\text{KL,shape}} = D_{\text{KL}}(p_*|p) \equiv \int d\vec{\lambda} p_* \ln p_*/p. \quad (18)$$

The KL divergence between a number of injected or observed events ( $\mu_*$ ) and an expected number of events ( $\mu$ ) can be derived from the Poisson distribution, and is simple to evaluate numerically:

$$D_{\text{KL,rate}} = D_{\text{KL}}(\mu_*|\mu) \equiv \mu_* - \mu + \mu \ln(\mu/\mu_*). \quad (19)$$

A measure of KL divergence informed by both rate and shape information must scale accordingly with  $\mu_*$ :

$$D_{\text{KL,joint}} = D_{\text{KL}}(p, \mu|p_*, \mu_*) \equiv D_{\text{KL}}(\mu_*|\mu) + \mu_* D_{\text{KL}}(p_*|p). \quad (20)$$

The KL divergence is positive semi-definite (it will be zero if and only if  $p = p_*$ ).

By constructing a functional form to represent the density of each population model, and integrating over the discrete set of samples which define observed population ( $p_*$ ), we can define a discretized KL divergence:

$$D_{\text{KL,shape}} = \frac{1}{\mu_*} \sum_k \ln(p_*(\vec{\lambda}_k)) - \ln(p(\vec{\lambda}_k)) \quad (21)$$

where  $p(\vec{\lambda}_k)$  and  $p_*(\vec{\lambda}_k)$  are approximations to the density of sample binaries which make up  $p$  and  $p_*$  respectively (The construction of which is deferred to Section

5.2). This is a Monte Carlo integration over samples from  $p_*$  (indexed by  $k$ ), and this sampling accounts for the factor of  $p_*$  outside the logarithm in Eq. 18.

### 5.2. Characterizing the Density of LISA-bright sources

When carrying out the Monte Carlo integration in Eq. 21, we must construct an approximation to the sample densities that make up  $p$  and  $p_*$ . These approximations take the form of a Gaussian mixture model, where  $p(\vec{\lambda}) = \sum_j \mathcal{L}_j(\vec{\lambda})/\mu$  and  $p_*(\vec{\lambda}) = \sum_{j^*} \mathcal{L}_{j^*}(\vec{\lambda})/\mu_*$ . Here,  $\mathcal{L}_j$  and  $\mathcal{L}_{j^*}$  are individual Gaussian components of the mixture model, and we construct them from the PE likelihood of each LISA-bright source (i.e. 12). We make the same SNR and  $f_{\text{GW}}$  cuts as in Section 4, and construct each population with the LISA-bright sample binaries. However, we make a modification by changing coordinates from  $f_{\text{GW}}$  to  $\log(f_{\text{GW}})$  in the construction of our density estimate. We also further inflate covariance estimates to define the width of each Gaussian component by a minimum of twice Scott's rule Scott (2015).

When sampling many galaxy realizations for each  $\alpha_{\text{CE}}$  value, we must choose a width for our Gaussian components which is wide enough so that the sampling error between realizations (sampled with different random number generator seeds) are not greater than the difference between our assumptions for  $\alpha_{\text{CE}}$ . While it may be possible to construct a mathematical method for choosing the width of Gaussian components to overcome this sampling error, we chose this value by hand in this work. The impact of individual samples from the test population on the KL divergence is also limited by setting a maximum contribution ( $\ln p/p_* \leq 1$ ) for individual samples to the integration in Eq. 21. As both the Inhomogeneous Poisson Point Process likelihood and KL divergence models require inflated covariances to at least Scott's rule, a detailed parameter estimation likelihood model may be unnecessary. As the KL divergence is more susceptible to sampling error, a likelihood-based approach may be preferable.

As a concrete example of this KL divergence approach Figure 7 shows the KL divergence between our Gaussian mixture models representing the injected CEB60 population and test populations with different  $\alpha_{\text{CE}}$ . In the top panel, we show the KL divergence calculated using only information about the expected number of events. In the second panel, we compute the KL divergence derived using only the DWD orbital parameter distributions  $p(\vec{\lambda})$ . In the third panel, we show an overall combination: In all three cases, the minimum value of the KL divergence occurs (as expected) near the true parameter value, even allowing for different galaxy realizations.

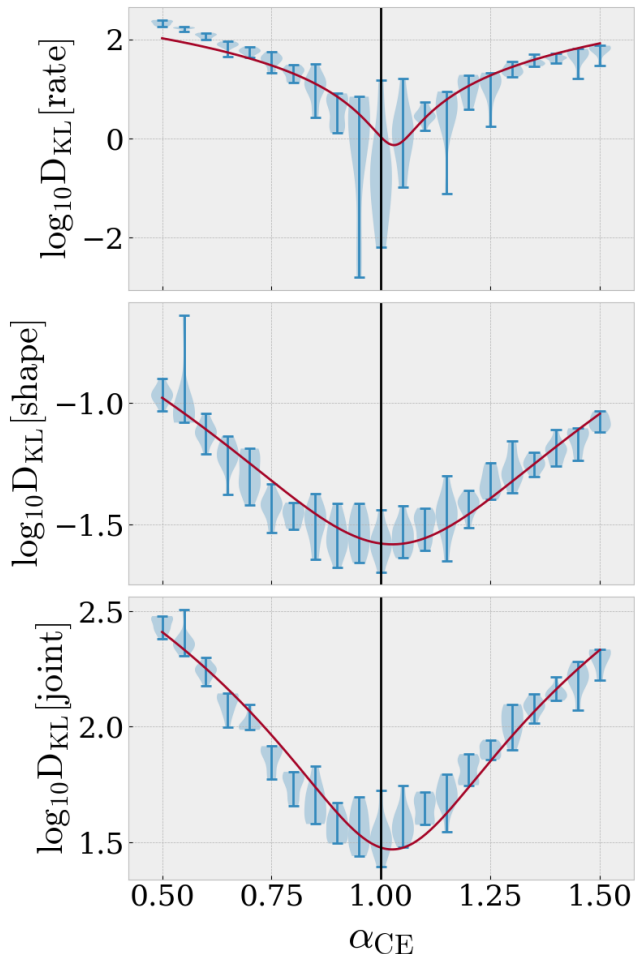


**Figure 7. The KL divergence in  $\alpha_{\text{CE}}$ :** Taking the same view as Figure 6, we see the components of the KL divergence attributed to Poisson error (top), the shape of the source distribution (middle), and both of these together (bottom). We note the presence of a few realizations for which the estimated KL divergence appears to be numerically unstable, despite our choices of coordinates and inflated Gaussian components.

### 5.3. A relationship between likelihood and KL divergence

To understand why the KL divergence and likelihood provide similar information, we review their expected relationship. This section is heavily inspired by O’Shaughnessy (2013).

Just as we are interested in finding the *more likely* model when using a maximum likelihood approach (rather than fixating on the value of a particular likelihood estimate), we are more interested here in the difference between KL divergence values for particular models (rather than the value of a particular KL divergence estimate). Any proposed realization of a “bootstrapped” reference population that approximates the samples be-

longing to  $p_*$  will predict on average  $\mu_*$  observations, with a distribution  $p_*$ , consistent with the injected population model. Following O’Shaughnessy (2013), the difference in KL divergence between the bootstrapped population and a given test population (characterized by  $\mu$  observations and a distribution of  $p$ ) are intimately related to the (expected) likelihood difference between the tested population model and injected population model. Averaging over possible realizations of the bootstrapped source population model, we find

$$\langle \ln P(\{d_j\}|\Lambda) \rangle = \langle \ln P(n|\mu) \rangle + \langle n \rangle \int d\vec{\lambda} p_*(\vec{\lambda}) \ln p(\vec{\lambda}). \quad (22)$$

where we note  $\langle n \rangle = \mu_*$ .

Reorganizing, we can express the difference in (expected) log likelihood between any two candidate populations  $(\mu_A, p_A)$  and  $(\mu_B, p_B)$  characterized by  $\Lambda_A$  and  $\Lambda_B$  in terms of differences in KL divergences:

$$-\langle \ln P(\{d_j\}|\Lambda_A) - \ln P(\{d_j\}|\Lambda_B) \rangle = \quad (23)$$

$$[\text{D}_{\text{KL}}(\mu_*|\mu_A) - \text{D}_{\text{KL}}(\mu_*|\mu_B)] + \mu_*[\text{D}_{\text{KL}}(p_*|p_A) - \text{D}_{\text{KL}}(p_*|p_B)]$$

In the special case that  $B$  is our mixture model approximating the (injected) reference population, then the likelihood difference will be zero if and only if  $A$  is also the bootstrapped reference population. Critically, we can therefore check if an estimated KL divergence and likelihood estimate agree with our understanding of their construction by dividing the left half of this equation by the right. If our model is well-constructed, the resulting expression should be consistent with unity.

Figure 8 validates this relationship, showing the close agreement between the rate likelihood and the Poisson KL divergence  $D_{\text{KL},\text{rate}}(\mu_*|\mu)$ ; the shape likelihood and the shape-only KL divergence  $\mu_* D_{\text{KL},\text{shape}}(p_*|p)$ ; and the overall likelihood and the “joint” KL divergence introduced above.

The key differences between this approach and the Inhomogeneous Poisson Point Process likelihood are:

- The KL divergence is sensitive to a difference between two models, rather than the agreement of a single model to a fixed set of observations (compare Eq. 18 and Eq. 13).
- In the likelihood approach, we only needed to construct a Gaussian mixture model for the injected population (not each test population). In the KL divergence approach,  $p$  and  $p_*$  are both evaluated using the functional form approximation (i.e. the bootstrapped model) from their own individual population samples.

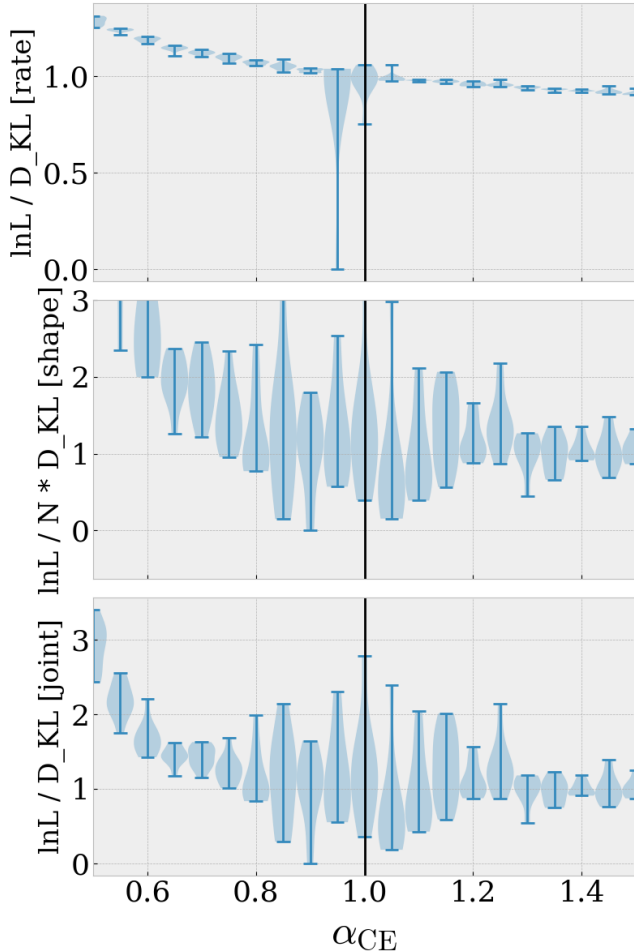


**Figure 8. Agreement of the KL divergence and log likelihood:** Taking the same view again as Figure 6, we measure the agreement of two methods of constraint: the log likelihood and KL divergence. As per Eq. 23, these values should be close to 1.0 if our model is well-constructed. We note that this is essentially true in the vicinity of the injected model ( $\alpha_{\text{CE}} = 1.0$ ).

## 6. HOW WELL IS AN INJECTION RECOVERED?

### 6.1. Estimating the Fisher uncertainty about formation parameters

A classic estimate for the measurement uncertainty of model hyperparameters  $\Lambda$  follows from a second-order expansion of the log-likelihood about its local maximum. In our context, a second-order expansion of the inhomogeneous Poisson log likelihood about the true parameters  $\Lambda_*$  produces an estimate of  $\Gamma_{ab}$ , the inverse covariance of the posterior distribution over the model hyperparameters  $\Lambda$ :

$$\ln P(\{d_j\}|\Lambda) \simeq \ln P(\{d_j\}|\Lambda_*) - \frac{1}{2} \Gamma_{ab} (\Lambda_a - \Lambda_{a,*}) (\Lambda_b - \Lambda_{b,*}). \quad (24)$$

Method	Component	$\langle \alpha_{\text{CE}} \rangle$	$\delta \alpha_{\text{CE}} \approx \sqrt{\Gamma_{\alpha\alpha}}$
lnP	Rate	1.093	0.096
lnP	Shape	1.012	0.072
lnP	Joint	1.019	0.052
$D_{\text{KL}}$	Rate	1.030	0.052
$D_{\text{KL}}$	Shape	1.026	0.053
$D_{\text{KL}}$	Joint	1.025	0.035

**Table 2. How well our common envelope assumption is recovered:** For the injected parameter ( $\alpha_{\text{CE}} = 1.0$ ), these are our Fisher uncertainties in an injection recovery study though the likelihood and KL divergence methods, considering the event rate and/or shape of the distribution.

For example, using the local polynomial approximations presented in Section 4, we can estimate  $\Gamma_{\alpha\alpha}$  for the full likelihood; see, e.g., Figure 6. Conversely, exploiting the duality between  $\ln P$  and  $D_{\text{KL}}$  established in Section 5, we can also estimate  $\Gamma_{ab}$  from a quadratic-order approximation to the KL divergence (see Eq. 15 of O’Shaughnessy 2013).

Table 2 exhibits the agreement of quadratic fits to the likelihood and KL divergence for each method with the injected value. Both methods provide a recovery the injected formation assumption for  $\alpha_{\text{CE}}$ , and the expected  $\alpha_{\text{CE}}$  value for each method agrees with the true value within 10%, and with each other method within the predicted error range (where  $\delta \alpha_{\text{CE}}$  is estimated by the Fisher value:  $\sqrt{\Gamma_{\alpha\alpha}}$ ).

## 7. DISCUSSION

In this work we have assessed the impact of common envelope evolution uncertainties on the population of DWDs that LISA may discover. We simulated 480 populations of DWDs across 15 metallicities and 32 common envelope ejection efficiencies using COSMIC. We then applied the metallicity-specific star formation history of The Milky-Way-like galaxy **m12i** from the FIRE-2 Latte Simulation Suite to create a synthetic Milky-Way-like population of DWDs. With this synthetic population, we investigated LISA’s ability to distinguish between models for the common envelope ejection efficiency using the measured strain and gravitational wave frequency evolution. Finally, we explored the potential for an Inhomogeneous Poisson point process likelihood to make those distinctions and compared with predictions made using a KL divergence approach, through both the number and properties of predicted detections.

We summarize our results as follows:

- The common envelope ejection efficiency,  $\alpha_{\text{CE}}$ , directly correlates with the *number* of DWDs that form per unit solar mass. As  $\alpha_{\text{CE}}$  increases, the

number of stellar mergers from failed common envelope ejections among the progenitors of DWD binaries decreases.

- The effects of changing the common envelope ejection efficiency are most prominently seen in the lowest mass stellar progenitors which produce He WD binaries since these systems are the most susceptible to failed common envelope ejections and subsequent stellar mergers.
- The effects of changing  $\alpha_{\text{CE}}$  mentioned above are also seen in the LISA Galactic DWD and LISA bright populations; however, the LISA bright population is less effected due to competition with the DWD confusion foreground.
- Both the Inhomogeneous Poisson point process likelihood and KL divergence statistics can be used to quantitatively distinguish between different models for DWD formation. We find that because the KL divergence method is more susceptible to sampling error, we recommend the Inhomogeneous Poisson Point Process likelihood for future population studies.
- Because inflated Gaussian covariances which are larger than PE uncertainties are required to overcome sampling error, we find that applying Scott's rule makes the Fisher estimates unnecessary.
- The strongest Bayesian inference constraints are found when constraining formation models with both the number and properties of LISA observable DWD systems. *The predicted number of detections alone may not be sufficient to distinguish between models.*
- When considering only changes to common envelope ejection efficiency, we find that LISA is sensitive at about the 10 % level. Future studies should consider how constraints change when incorporating other uncertain models (E.g. different common envelope models, mass transfer stability).

By demonstrating a recovery of the underlying astrophysical assumptions in a one-dimensional population model, we have demonstrated a method of learning about the isolated binary evolution formation channel for close DWD binaries. Based on our recovery of the common envelope efficiency parameter, we conclude that common envelope physics are a good target for future studies of binary population synthesis studies when real LISA observations are recorded. We also demonstrate

a method of using Bayesian hierarchical inference methods popularized for current studies of LVK observations to constrain LISA DWDs.

In addition to the bright DWD population, LISA may observe a population of neutron star white dwarf binaries (Nelemans et al. 2001; Moore et al. 2023; Korol et al. 2023), stellar mass black hole binaries during inspiral (Sesana 2016), and stochastic gravitational wave Galactic foreground (Karnesis et al. 2021). It may be possible to learn about the formation and evolution of binary stars from these binaries as well. Future work may explore the impact of these potential sources on population inference.

By studying various formation assumptions for the LISA Galactic DWD binaries, we not only prepare ourselves for future investigations of LISA observable populations, but we also create tools for constructing synthetic populations of LISA DWD binaries for a given choice of assumptions for use in other contexts. One such example is the LISA global fit pipeline (Littenberg & Cornish 2023; Gao et al. 2023; Finch et al. 2023; Lackeos et al. 2023; Katz et al. 2024; Strub et al. 2024). Many such pipelines have been using the same DWD populations for a long time. In collaboration with these efforts our work can both provide simulation tools to support DWD inference pipeline and catalog development and can begin prototyping end-to-end hierarchical inference analyses needed to better understand the physical processes which produce DWDs.

*Data/Code availability*—A limited set of data supporting the findings of this study is openly available at <https://zenodo.org/records/13872540> (Delfavero et al. 2024a). The code supporting the findings of this study is available at <https://zenodo.org/records/14421368> (Delfavero et al. 2024b).

1 The authors thank Ann E. Hornschemeier and the  
 2 anonymous referee for useful proofreading and feed-  
 3 back. VD is supported by an appointment to the NASA  
 4 Postdoctoral Program at the NASA Goddard Space  
 5 Flight Center administered by Oak Ridge Associated  
 6 Universities under contract NPP-GSFC-NOV21-0031.  
 7 ROS gratefully acknowledges support from NSF awards  
 8 NSF PHY-1912632, PHY-2012057, PHY-2309172, AST-  
 9 2206321, and the Simons Foundation. JB is supported  
 10 by the NASA LISA Project Office.

11 We acknowledge software packages used in this publi-  
 12 cation, including NUMPY (Harris et al. 2020), SCIPY  
 13 (Virtanen et al. 2020), MATPLOTLIB (Hunter 2007),  
 14 ASTROPY (Astropy Collaboration et al. 2013, 2018; ast  
 15 2022), H5PY (Collette 2013), LEGWORK (Wagg et al.  
 16 2022), and ldssoft Littenberg et al. (2020). This research  
 17 was done using resources provided by the Open Science  
 18 Grid (Pordes et al. 2007; Sfiligoi et al. 2009), which is  
 19 supported by the National Science Foundation awards  
 20 #2030508 and #1836650, and the U.S. Department of  
 21 Energy’s Office of Science.

## REFERENCES

- 2022, 935, 167, doi: [10.3847/1538-4357/ac7c74](https://doi.org/10.3847/1538-4357/ac7c74)
- Abbott, B., Abbott, R., Abbott, T., Abernathy, M., & et al. 2016, *Physical Review D*, 93, doi: [10.1103/physrevd.93.122003](https://doi.org/10.1103/physrevd.93.122003)
- Abbott, B., Abbott, R., Abbott, T., Abraham, S., & et al. 2019, *Physical Review X*, 9, 031040
- Abbott, R., Abbott, T., Abraham, S., Acernese, F., & et al. 2021a, *Physical Review X*, 11, 021053
- Abbott, R., Abbott, T. D., Abraham, S., & et al., F. A. 2021b, *The Astrophysical Journal Letters*, 915, L5, doi: [10.3847/2041-8213/ac082e](https://doi.org/10.3847/2041-8213/ac082e)
- Anders, E., & Grevesse, N. 1989, *Geochimica et Cosmochimica Acta*, 53, 197, doi: [10.1016/0016-7037\(89\)90286-X](https://doi.org/10.1016/0016-7037(89)90286-X)
- Ashton, G., Hübner, M., Lasky, P. D., et al. 2019, *The Astrophysical Journal Supplement Series*, 241, 27, doi: [10.3847/1538-4365/ab06fc](https://doi.org/10.3847/1538-4365/ab06fc)
- Asplund, M., Grevesse, N., Sauval, A. J., & Scott, P. 2009, *ARA&A*, 47, 481, doi: [10.1146/annurev.astro.46.060407.145222](https://doi.org/10.1146/annurev.astro.46.060407.145222)
- Astropy Collaboration, Price-Whelan, A. M., Sipőcz, B. M., Günther, H. M., & et al. 2018, *Astronomical Journal*, 156, 123, doi: [10.3847/1538-3881/aabc4f](https://doi.org/10.3847/1538-3881/aabc4f)
- Astropy Collaboration, Robitaille, T. P., Tollerud, E. J., Greenfield, P., & et al. 2013, *A&A*, 558, A33, doi: [10.1051/0004-6361/201322068](https://doi.org/10.1051/0004-6361/201322068)
- Barrett, J. W., Gaebel, S. M., Neijssel, C. J., et al. 2017, *Monthly Notices of the Royal Astronomical Society*, doi: [10.1093/mnras/sty908](https://doi.org/10.1093/mnras/sty908)
- Belczynski, K., Klencki, J., Fields, C. E., Olejak, A., & et al. 2020, *Astronomy & Astrophysics*, 636, A104, doi: [10.1051/0004-6361/201936528](https://doi.org/10.1051/0004-6361/201936528)
- Benacquista, M., & Holley-Bockelmann, K. 2006, *Astrophysical Journal*, 645, 589, doi: [10.1086/504024](https://doi.org/10.1086/504024)
- Biscoveanu, S., Kremer, K., & Thrane, E. 2023, *The Astrophysical Journal*, 949, 95, doi: [10.3847/1538-4357/acc585](https://doi.org/10.3847/1538-4357/acc585)
- Breivik, K., Coughlin, S., Zevin, M., Rodriguez, C. L., & et al. 2020, *The Astrophysical Journal*, 898, 71, doi: [10.3847/1538-4357/ab9d85](https://doi.org/10.3847/1538-4357/ab9d85)
- Breivik, K., Kremer, K., Bueno, M., et al. 2018, *The Astrophysical Journal Letters*, 854, L1, doi: [10.3847/2-041-8213/aaaa23](https://doi.org/10.3847/2-041-8213/aaaa23)
- Breivik, K., Mingarelli, C. M. F., & Larson, S. L. 2020, *Astrophysical Journal*, 901, 4, doi: [10.3847/1538-4357/abab99](https://doi.org/10.3847/1538-4357/abab99)
- Breivik, K., Coughlin, S., Zevin, M., et al. 2021, COSMIC: Compact Object Synthesis and Monte Carlo Investigation Code, *Astrophysics Source Code Library*, record ascl:2108.022
- Broekgaarden, F. S., & Berger, E. 2021, *The Astrophysical Journal Letters*, 920, L13



- Broekgaarden, F. S., Berger, E., Stevenson, S., et al. 2021, arXiv preprint arXiv:2112.05763
- Broekgaarden, F. S., Justham, S., de Mink, S. E., et al. 2019, MNRAS, 490, 5228, doi: [10.1093/mnras/stz2558](https://doi.org/10.1093/mnras/stz2558)
- Callister, T. A. 2021, arXiv e-prints, arXiv:2104.09508. <https://arxiv.org/abs/2104.09508>
- Claeys, J. S. W., Pols, O. R., Izzard, R. G., Vink, J., & Verbunt, F. W. M. 2014, A&A, 563, A83, doi: [10.1051/0004-6361/201322714](https://doi.org/10.1051/0004-6361/201322714)
- Collaboration, L. S., & Collaboration, V. 2021, GWTC-2.1: Deep Extended Catalog of Compact Binary Coalescences Observed by LIGO and Virgo During the First Half of the Third Observing Run - Parameter Estimation Data Release, v2, Zenodo, doi: [10.5281/zenodo.6513631](https://doi.org/10.5281/zenodo.6513631)
- Collaboration, L. S., Collaboration, V., & Collaboration, K. 2021, GWTC-3: Compact Binary Coalescences Observed by LIGO and Virgo During the Second Part of the Third Observing Run — Parameter estimation data release, Zenodo, doi: [10.5281/zenodo.5546663](https://doi.org/10.5281/zenodo.5546663)
- Collette, A. 2013, Python and HDF5 (O'Reilly)
- Colpi, M., Danzmann, K., Hewitson, M., et al. 2024, arXiv e-prints, arXiv:2402.07571, doi: [10.48550/arXiv.2402.07571](https://doi.org/10.48550/arXiv.2402.07571)
- Cutler, C., & Flanagan, E. E. 1994, Phys. Rev. D, 49, 2658, doi: [10.1103/PhysRevD.49.2658](https://doi.org/10.1103/PhysRevD.49.2658)
- De Marco, O., Passy, J.-C., Moe, M., et al. 2011, MNRAS, 411, 2277, doi: [10.1111/j.1365-2966.2010.17891.x](https://doi.org/10.1111/j.1365-2966.2010.17891.x)
- Delfavero, V., Breivik, K., Thiele, S., O'Shaughnessy, R., & Baker, J. 2024a, Galactic Populations of LISA DWD Binaries, 1.0, Zenodo, doi: [10.5281/zenodo.13872540](https://doi.org/10.5281/zenodo.13872540)
- . 2024b, BASIL - COSMIC, 1.0, Zenodo, doi: [10.5281/zenodo.14421368](https://doi.org/10.5281/zenodo.14421368)
- Delfavero, V., O'Shaughnessy, R., Belczynski, K., Drozda, P., & Wysocki, D. 2023, Phys. Rev. D, 108, 043023, doi: [10.1103/PhysRevD.108.043023](https://doi.org/10.1103/PhysRevD.108.043023)
- Delfavero, V., O'Shaughnessy, R., Wysocki, D., & Yelikar, A. 2021, Normal Approximate Likelihoods to Gravitational Wave Events, arXiv, doi: [10.48550/ARXIV.2107.13082](https://doi.org/10.48550/ARXIV.2107.13082)
- . 2022, Compressed Parametric and Non-Parametric Approximations to the Gravitational Wave Likelihood, arXiv, doi: [10.48550/ARXIV.2205.14154](https://doi.org/10.48550/ARXIV.2205.14154)
- Eldridge, J. J., Stanway, E. R., Xiao, L., et al. 2017, Publications of the Astronomical Society of Australia, 34, e058, doi: [10.1017/pasa.2017.51](https://doi.org/10.1017/pasa.2017.51)
- eLISA Consortium et al., T. 2013, The Gravitational Universe. <https://arxiv.org/abs/1305.5720>
- Fabbiano, G. 2006, ARA&A, 44, 323, doi: [10.1146/annurev.astro.44.051905.092519](https://doi.org/10.1146/annurev.astro.44.051905.092519)
- Finch, E., Bartolucci, G., Chucherko, D., et al. 2023, MNRAS, 522, 5358, doi: [10.1093/mnras/stad1288](https://doi.org/10.1093/mnras/stad1288)
- Flournoy, N., & Tsutakawa, R. K. 1991, Statistical Multiple Integration: Proceedings of a Joint Summer Research Conference Held at Humboldt University, June 17-23, 1989, Vol. 115 (American Mathematical Soc.)
- Fortin, Francis, García, Federico, Simaz Bunzel, Adolfo, & Chaty, Sylvain. 2023, A&A, 671, A149, doi: [10.1051/0004-6361/202245236](https://doi.org/10.1051/0004-6361/202245236)
- Fragione, G., Loeb, A., & Rasio, F. A. 2020, The Astrophysical Journal, 902, L26, doi: [10.3847/2041-8213/abbc0a](https://doi.org/10.3847/2041-8213/abbc0a)
- Fragos, T., Andrews, J. J., Bavera, S. S., et al. 2022, POSYDON: A General-Purpose Population Synthesis Code with Detailed Binary-Evolution Simulations. <https://arxiv.org/abs/2202.05892>
- Frohmaier, C., Sullivan, M., Maguire, K., & Nugent, P. 2018, Astrophysical Journal, 858, 50, doi: [10.3847/1538-4357/aabc0b](https://doi.org/10.3847/1538-4357/aabc0b)
- Gamba, R., Breschi, M., Carullo, G., et al. 2023, Nature Astronomy, 7, 11, doi: [10.1038/s41550-022-01813-w](https://doi.org/10.1038/s41550-022-01813-w)
- Gao, P., Fan, X.-L., Cao, Z.-J., & Zhang, X.-H. 2023, Phys. Rev. D, 107, 123029, doi: [10.1103/PhysRevD.107.123029](https://doi.org/10.1103/PhysRevD.107.123029)
- Garrison-Kimmel, S., Wetzel, A., Bullock, J. S., et al. 2017, MNRAS, 471, 1709, doi: [10.1093/mnras/stx1710](https://doi.org/10.1093/mnras/stx1710)
- Gayathri, V., Healy, J., Lange, J., et al. 2022, Nature Astronomy, 6, 344–349, doi: <https://doi.org/10.1038/s41550-021-01568-w>
- Giacobbo, N., Mapelli, M., & Spera, M. 2017, Monthly Notices of the Royal Astronomical Society, 474, 2959, doi: [10.1093/mnras/stx2933](https://doi.org/10.1093/mnras/stx2933)
- Giacobbo, N., Mapelli, M., & Spera, M. 2018, MNRAS, 474, 2959, doi: [10.1093/mnras/stx2933](https://doi.org/10.1093/mnras/stx2933)
- Gokhale, V., Peng, X. M., & Frank, J. 2007, Astrophysical Journal, 655, 1010, doi: [10.1086/510119](https://doi.org/10.1086/510119)
- Harris, C. R., Millman, K. J., van der Walt, S. J., Gommers, R., & et al. 2020, Nature, 585, 357, doi: [10.1038/s41586-020-2649-2](https://doi.org/10.1038/s41586-020-2649-2)
- Hirai, R., & Mandel, I. 2022, The Astrophysical Journal Letters, 937, L42, doi: [10.3847/2041-8213/ac9519](https://doi.org/10.3847/2041-8213/ac9519)
- Hofman, S., & Nelemans, G. 2024, arXiv e-prints, arXiv:2407.10642, doi: [10.48550/arXiv.2407.10642](https://doi.org/10.48550/arXiv.2407.10642)
- Hopkins, P. F. 2015, Monthly Notices of the Royal Astronomical Society, 450, 53, doi: [10.1093/mnras/stv195](https://doi.org/10.1093/mnras/stv195)
- Hopkins, P. F., Kereš, D., Oñorbe, J., et al. 2014, Monthly Notices of the Royal Astronomical Society, 445, 581, doi: [10.1093/mnras/stu1738](https://doi.org/10.1093/mnras/stu1738)
- Hopkins, P. F., Wetzel, A., Kereš, D., et al. 2018, MNRAS, 480, 800, doi: [10.1093/mnras/sty1690](https://doi.org/10.1093/mnras/sty1690)

- Hunter, J. D. 2007, *Computing in Science & Engineering*, 9, 90, doi: [10.1109/MCSE.2007.55](https://doi.org/10.1109/MCSE.2007.55)
- Hurley, J. R., Pols, O. R., & Tout, C. A. 2000, *Monthly Notices of the Royal Astronomical Society*, 315, 543, doi: [10.1046/j.1365-8711.2000.03426.x](https://doi.org/10.1046/j.1365-8711.2000.03426.x)
- Hurley, J. R., Tout, C. A., & Pols, O. R. 2002, *Monthly Notices of the Royal Astronomical Society*, 329, 897, doi: [10.1046/j.1365-8711.2002.05038.x](https://doi.org/10.1046/j.1365-8711.2002.05038.x)
- Inoue, Y., Yabe, K., & Ueda, Y. 2022, *VizieR Online Data Catalog: Extragalactic X-ray binaries catalog (Inoue+, 2021)*, *VizieR On-line Data Catalog: J/PASJ/73/1315*. Originally published in: 2021PASJ...73.1315I
- Ivanova, N. 2011, *The Astrophysical Journal*, 730, 76, doi: [10.1088/0004-637x/730/2/76](https://doi.org/10.1088/0004-637x/730/2/76)
- Ivanova, N., & Chaichenets, S. 2011, *The Astrophysical Journal*, 731, L36, doi: [10.1088/2041-8205/731/2/L36](https://doi.org/10.1088/2041-8205/731/2/L36)
- Karnesis, N., Babak, S., Pieroni, M., Cornish, N., & Littenberg, T. 2021, *Phys. Rev. D*, 104, 043019, doi: [10.1103/PhysRevD.104.043019](https://doi.org/10.1103/PhysRevD.104.043019)
- Katz, M. L., Karnesis, N., Korsakova, N., Gair, J. R., & Stergioulas, N. 2024, *arXiv e-prints*, arXiv:2405.04690, doi: [10.48550/arXiv.2405.04690](https://doi.org/10.48550/arXiv.2405.04690)
- Keim, M. A., Korol, V., & Rossi, E. M. 2023, *MNRAS*, 521, 1088, doi: [10.1093/mnras/stad554](https://doi.org/10.1093/mnras/stad554)
- Klencki, J., Nelemans, G., Istrate, A. G., & Chruslinska, M. 2021, *Astronomy & Astrophysics*, 645, A54, doi: [10.1051/0004-6361/202038707](https://doi.org/10.1051/0004-6361/202038707)
- Korol, V., Belokurov, V., & Toonen, S. 2022a, *Monthly Notices of the Royal Astronomical Society*, 515, 1228, doi: [10.1093/mnras/stac1686](https://doi.org/10.1093/mnras/stac1686)
- Korol, V., Hallakoun, N., Toonen, S., & Karnesis, N. 2022b, *Monthly Notices of the Royal Astronomical Society*, 511, 5936, doi: [10.1093/mnras/stac415](https://doi.org/10.1093/mnras/stac415)
- Korol, V., Igoshev, A. P., Toonen, S., et al. 2023, *Neutron Star - White Dwarf Binaries: Probing Formation Pathways and Natal Kicks with LISA*. <https://arxiv.org/abs/2310.06559>
- Korol, V., Koop, O., & Rossi, E. M. 2018, *Astrophysical Journal*, 866, L20, doi: [10.3847/2041-8213/aae587](https://doi.org/10.3847/2041-8213/aae587)
- Korol, V., Rossi, E. M., & Barausse, E. 2018, *Monthly Notices of the Royal Astronomical Society*, 483, 5518, doi: [10.1093/mnras/sty3440](https://doi.org/10.1093/mnras/sty3440)
- Korol, V., Rossi, E. M., Groot, P. J., et al. 2017, *Monthly Notices of the Royal Astronomical Society*, 470, 1894, doi: [10.1093/mnras/stx1285](https://doi.org/10.1093/mnras/stx1285)
- Korol, V., Toonen, S., Klein, A., et al. 2020, *A&A*, 638, A153, doi: [10.1051/0004-6361/202037764](https://doi.org/10.1051/0004-6361/202037764)
- Kremer, K., Breivik, K., Larson, S. L., & Kalogera, V. 2017, *The Astrophysical Journal*, 846, 95, doi: [10.3847/1538-4357/aa8557](https://doi.org/10.3847/1538-4357/aa8557)
- Kremer, K., Chatterjee, S., Breivik, K., et al. 2018, *Phys. Rev. Lett*, 120, 191103, doi: [10.1103/PhysRevLett.120.191103](https://doi.org/10.1103/PhysRevLett.120.191103)
- Kremer, K., Rui, N. Z., Weatherford, N. C., et al. 2021, *Astrophysical Journal*, 917, 28, doi: [10.3847/1538-4357/ac06d4](https://doi.org/10.3847/1538-4357/ac06d4)
- Kremer, K., Sepinsky, J., & Kalogera, V. 2015, *Astrophysical Journal*, 806, 76, doi: [10.1088/0004-637X/806/1/76](https://doi.org/10.1088/0004-637X/806/1/76)
- Kremer, K., Ye, C. S., Rui, N. Z., et al. 2020, *ApJS*, 247, 48, doi: [10.3847/1538-4365/ab7919](https://doi.org/10.3847/1538-4365/ab7919)
- Kroupa, P., & Weidner, C. 2003, *The Astrophysical Journal*, 598, 1076, doi: [10.1086/379105](https://doi.org/10.1086/379105)
- Kullback. 1959, *Information theory and statistics* (John Wiley and Sons, NY)
- Lackeos, K., Littenberg, T. B., Cornish, N. J., & Thorpe, J. I. 2023, *A&A*, 678, A123, doi: [10.1051/0004-6361/202347222](https://doi.org/10.1051/0004-6361/202347222)
- Lamberts, A., Blunt, S., Littenberg, T. B., et al. 2019, *MNRAS*, 490, 5888, doi: [10.1093/mnras/stz2834](https://doi.org/10.1093/mnras/stz2834)
- Littenberg, T., Cornish, N., Lackeos, K., & Robson, T. 2020, *tlittenberg/ldasoft: GBMCMC v1.0.1, 1.0.1*, Zenodo, doi: [10.5281/zenodo.3756199](https://doi.org/10.5281/zenodo.3756199)
- Littenberg, T. B., & Cornish, N. J. 2023, *Phys. Rev. D*, 107, 063004, doi: [10.1103/PhysRevD.107.063004](https://doi.org/10.1103/PhysRevD.107.063004)
- Mandel, I., & Farmer, A. 2022, *Physics Reports*, 955, 1, doi: <https://doi.org/10.1016/j.physrep.2022.01.003>
- Marsh, T. R., Nelemans, G., & Steeghs, D. 2004, *MNRAS*, 350, 113, doi: [10.1111/j.1365-2966.2004.07564.x](https://doi.org/10.1111/j.1365-2966.2004.07564.x)
- Miller-Jones, J. C. A. 2014, *Publications of the Astronomical Society of Australia*, 31, e016, doi: [10.1017/pasa.2014.7](https://doi.org/10.1017/pasa.2014.7)
- Moe, M., Kratter, K. M., & Badenes, C. 2019, *The Astrophysical Journal*, 875, 61, doi: [10.3847/1538-4357/ab0d88](https://doi.org/10.3847/1538-4357/ab0d88)
- Moller, J., & Waagepetersen, R. P. 2003, *Statistical inference and simulation for spatial point processes* (CRC press)
- Moore, C. J., Finch, E., Klein, A., et al. 2023, *Discovering neutron stars with LISA via measurements of orbital eccentricity in Galactic binaries*. <https://arxiv.org/abs/2310.06568>
- Nelemans, G., Yungelson, L. R., & Portegies Zwart, S. F. 2001, *A&A*, 375, 890, doi: [10.1051/0004-6361:20010683](https://doi.org/10.1051/0004-6361:20010683)
- Nissanke, S., Vallisneri, M., Nelemans, G., & Prince, T. A. 2012, *Astrophysical Journal*, 758, 131, doi: [10.1088/0004-637X/758/2/131](https://doi.org/10.1088/0004-637X/758/2/131)

- Offner, S. S. R., Moe, M., Kratter, K. M., et al. 2023, in *Astronomical Society of the Pacific Conference Series*, Vol. 534, *Protostars and Planets VII*, ed. S. Inutsuka, Y. Aikawa, T. Muto, K. Tomida, & M. Tamura, 275, doi: [10.48550/arXiv.2203.10066](https://doi.org/10.48550/arXiv.2203.10066)
- O’Shaughnessy, R. 2013, *Phys. Rev. D*, 88, 084061, doi: [10.1103/PhysRevD.88.084061](https://doi.org/10.1103/PhysRevD.88.084061)
- Paczynski, B. 1976, in *Structure and Evolution of Close Binary Systems*, ed. P. Eggleton, S. Mitton, & J. Whelan, Vol. 73, 75
- Peters, P. C. 1964, *Phys. Rev.*, 136, B1224, doi: [10.1103/PhysRev.136.B1224](https://doi.org/10.1103/PhysRev.136.B1224)
- Pols, O. R., Schröder, K.-P., Hurley, J. R., Tout, C. A., & Eggleton, P. P. 1998, *MNRAS*, 298, 525, doi: [10.1046/j.1365-8711.1998.01658.x](https://doi.org/10.1046/j.1365-8711.1998.01658.x)
- Pordes, R., Petravick, D., Kramer, B., et al. 2007, in 78, Vol. 78, *J. Phys. Conf. Ser.*, 012057, doi: [10.1088/1742-6596/78/1/012057](https://doi.org/10.1088/1742-6596/78/1/012057)
- Portegies Zwart, S. F., & Verbunt, F. 1996, *A&A*, 309, 179
- Remillard, R. A., & McClintock, J. E. 2006, *Annual Review of Astronomy and Astrophysics*, 44, 49–92, doi: [10.1146/annurev.astro.44.051905.092532](https://doi.org/10.1146/annurev.astro.44.051905.092532)
- Riley, J., Agrawal, P., Barrett, J. W., et al. 2022, *ApJS*, 258, 34, doi: [10.3847/1538-4365/ac416c](https://doi.org/10.3847/1538-4365/ac416c)
- Roebber, E., Buscicchio, R., Vecchio, A., et al. 2020, *Astrophysical Journal*, 894, L15, doi: [10.3847/2041-8213/ab8ac9](https://doi.org/10.3847/2041-8213/ab8ac9)
- Romero-Shaw, I. M., Lasky, P. D., Thrane, E., & Bustillo, J. C. 2020, *The Astrophysical Journal Letters*, doi: [10.3847/2041-8213/abbe26](https://doi.org/10.3847/2041-8213/abbe26)
- Ruiter, A. J., Belczynski, K., Benacquista, M., Larson, S. L., & Williams, G. 2010, *The Astrophysical Journal*, 717, 1006, doi: [10.1088/0004-637X/717/2/1006](https://doi.org/10.1088/0004-637X/717/2/1006)
- Sanderson, R. E., Wetzel, A., Loebman, S., et al. 2020, *The Astrophysical Journal Supplement Series*, 246, 6, doi: [10.3847/1538-4365/ab5b9d](https://doi.org/10.3847/1538-4365/ab5b9d)
- Scherbak, P., & Fuller, J. 2023, *MNRAS*, 518, 3966, doi: [10.1093/mnras/stac3313](https://doi.org/10.1093/mnras/stac3313)
- Scott, D. W. 2015, *Multivariate density estimation: theory, practice, and visualization* (John Wiley & Sons)
- Sepinsky, J. F., Willems, B., Kalogera, V., & Rasio, F. A. 2010, *Astrophysical Journal*, 724, 546, doi: [10.1088/0004-637X/724/1/546](https://doi.org/10.1088/0004-637X/724/1/546)
- Sesana, A. 2016, *Phys. Rev. Lett.*, 116, 231102, doi: [10.1103/PhysRevLett.116.231102](https://doi.org/10.1103/PhysRevLett.116.231102)
- Sfiligoi, I., Bradley, D. C., Holzman, B., et al. 2009, in 2, Vol. 2, 2009 WRI World Congress on Computer Science and Information Engineering, 428–432, doi: [10.1109/CSIE.2009.950](https://doi.org/10.1109/CSIE.2009.950)
- Staelens, S., & Nelemans, G. 2024, *A&A*, 683, A139, doi: [10.1051/0004-6361/202348429](https://doi.org/10.1051/0004-6361/202348429)
- Stefano, R. D., Kruckow, M. U., Gao, Y., Neunteufel, P. G., & Kobayashi, C. 2023, *The Astrophysical Journal*, 944, 87, doi: [10.3847/1538-4357/acae9b](https://doi.org/10.3847/1538-4357/acae9b)
- Stevenson, S., Berry, C. P. L., & Mandel, I. 2017, *MNRAS*, 471, 2801, doi: [10.1093/mnras/stx1764](https://doi.org/10.1093/mnras/stx1764)
- Stevenson, S., & Clarke, T. A. 2022, *Monthly Notices of the Royal Astronomical Society*, 517, 4034
- Strub, S. H., Ferraioli, L., Schmelzbach, C., Stähler, S. C., & Giardini, D. 2024, *Phys. Rev. D*, 110, 024005, doi: [10.1103/PhysRevD.110.024005](https://doi.org/10.1103/PhysRevD.110.024005)
- Tang, P., Eldridge, J. J., Meyer, R., et al. 2024, *MNRAS*, 534, 1707, doi: [10.1093/mnras/stae2154](https://doi.org/10.1093/mnras/stae2154)
- The LIGO Scientific Collaboration, & The Virgo Collaboration. 2021, *GWTC-2.1: Deep Extended Catalog of Compact Binary Coalescences Observed by LIGO and Virgo During the First Half of the Third Observing Run*. <https://arxiv.org/abs/2108.01045>
- The LIGO Scientific Collaboration, The Virgo Collaboration, & The KAGRA Collaboration. 2020, Available as LIGO-P2000077. <https://dcc.ligo.org/LIGO-P2000077>
- . 2021a, *GWTC-3: Compact Binary Coalescences Observed by LIGO and Virgo During the Second Part of the Third Observing Run*. <https://arxiv.org/abs/2111.03606>
- . 2021b, *The population of merging compact binaries inferred using gravitational waves through GWTC-3*. <https://arxiv.org/abs/2111.03634>
- Thiele, S., Breivik, K., Sanderson, R. E., & Luger, R. 2023, *The Astrophysical Journal*, 945, 162, doi: [10.3847/1538-4357/aca7be](https://doi.org/10.3847/1538-4357/aca7be)
- Toonen, S., Nelemans, G., & Portegies Zwart, S. 2012, *A&A*, 546, A70, doi: [10.1051/0004-6361/201218966](https://doi.org/10.1051/0004-6361/201218966)
- Tout, C. A., Pols, O. R., Eggleton, P. P., & Han, Z. 1996, *MNRAS*, 281, 257, doi: [10.1093/mnras/281.1.257](https://doi.org/10.1093/mnras/281.1.257)
- Vallisneri, M. 2008, *Phys. Rev. D*, 77, 042001, doi: [10.1103/PhysRevD.77.042001](https://doi.org/10.1103/PhysRevD.77.042001)
- Veitch, J., Raymond, V., Farr, B., et al. 2015, *Phys. Rev. D*, 91, 042003, doi: [10.1103/PhysRevD.91.042003](https://doi.org/10.1103/PhysRevD.91.042003)
- Virtanen, P., Gommers, R., Oliphant, T. E., et al. 2020, *Nature Methods*, 17, 261, doi: [10.1038/s41592-019-0686-2](https://doi.org/10.1038/s41592-019-0686-2)
- Wagg, T., Breivik, K., & de Mink, S. 2022, *The Journal of Open Source Software*, 7, 3998, doi: [10.21105/joss.03998](https://doi.org/10.21105/joss.03998)
- Wetzel, A. R., Hopkins, P. F., Kim, J.-h., et al. 2016, *Astrophysical Journal*, 827, L23, doi: [10.3847/2041-8205/827/2/L23](https://doi.org/10.3847/2041-8205/827/2/L23)
- Willems, B., Kalogera, V., Vecchio, A., et al. 2007, *Astrophysical Journal*, 665, L59, doi: [10.1086/521049](https://doi.org/10.1086/521049)

- Wilson, E. C., & Nordhaus, J. 2022, arXiv e-prints, arXiv:2203.06091. <https://arxiv.org/abs/2203.06091>
- Wysocki, D., Lange, J., & O'Shaughnessy, R. 2019, Physical Review D, 100, doi: [10.1103/physrevd.100.043012](https://doi.org/10.1103/physrevd.100.043012)
- Yamaguchi, N., El-Badry, K., Rees, N., et al. 2024a, arXiv e-prints, arXiv:2405.06020, doi: [10.48550/arXiv.2405.06020](https://doi.org/10.48550/arXiv.2405.06020)
- Yamaguchi, N., El-Badry, K., Fuller, J., et al. 2024b, MNRAS, 527, 11719, doi: [10.1093/mnras/stad4005](https://doi.org/10.1093/mnras/stad4005)
- Zevin, M., Bavera, S. S., Berry, C. P. L., et al. 2021, Astrophysical Journal, 910, 152, doi: [10.3847/1538-4357/abe40e](https://doi.org/10.3847/1538-4357/abe40e)
- Zorotovic, M., Schreiber, M. R., Gänsicke, B. T., & Nebot Gómez-Morán, A. 2010, A&A, 520, A86, doi: [10.1051/0004-6361/200913658](https://doi.org/10.1051/0004-6361/200913658)